**INVESTIGATION OF THE PERFORMANCE
CHARACTERISTICS OF RE-ENTRY VEHICLES**

THESIS

Charles A. Bilbey, SMSgt, USAF

AFIT/GSS/ENY/05-S01

**DEPARTMENT OF THE AIR FORCE
AIR UNIVERSITY**

AIR FORCE INSTITUTE OF TECHNOLOGY

Wright-Patterson Air Force Base, Ohio

APPROVED FOR PUBLIC RELEASE; DISTRIBUTION UNLIMITED

INVESTIGATION OF THE PERFORMANCE
CHARACTERISTICS OF RE-ENTRY VEHICLES

THESIS

Presented to the Faculty

Department of Aeronautics and Astronautics

Graduate School of Engineering and Management

Air Force Institute of Technology

Air University

Air Education and Training Command

In Partial Fulfillment of the Requirements for the

Degree of Master of Science (Space Systems)

Charles A. Bilbey

SMSgt, USAF

September 2005

**INVESTIGATION OF THE PERFORMANCE
CHARACTERISTICS OF RE-ENTRY VEHICLES**

Charles A. Bilbey

SMSgt, USAF

Approved:

_____   _____
Dr. Richard G. Cobb (Chairman)   Date

_____   _____
Kerry D. Hicks, Lt Col, USAF (Member)   Date

_____   _____
Dr. Bradley S. Liebst (Member)   Date

Abstract

The "maneuverable re-entry vehicle" concept involves a re-entry vehicle capable of performing preplanned flight maneuvers during the re-entry phase. This study investigated the atmospheric re-entry profiles of a maneuverable re-entry vehicle. The re-entry vehicle was modeled as a point mass with aerodynamic properties. Equations of motion were identified as derived by Nguyen Vinh, and the system of equations numerically integrated, giving the time histories of position, velocity and flight path angle. The algorithm is able to generate a complete and feasible entry trajectory of approximately 25-minute flight time in about 5 to 10 seconds on a desktop computer, given the entry conditions and values of constraint parameters. The concept of modeling a re-entry trajectory using MATLAB software is an effective method for predicting the flight characteristics of an unknown vehicle entering the earth's atmosphere. Although the entry altitude was chosen to be 122 km, atmospheric effects are essentially negligible until the vehicle reaches an altitude near 80 km. Until 80 km altitude, the velocity and flight path angle remain essentially constant. This preliminary study shows the feasibility of identifying and further exploring the technical challenges involved in using a mathematical model to simulate the performance characteristics of an unknown re-entry vehicle.

Acknowledgments

I would like to express appreciation to my faculty advisor, Dr. Richard Cobb, for his support and guidance throughout the course of this research effort. I would also like to thank Lt. Col. (Dr) Kerry Hicks for agreeing to teach the Atmospheric Re-entry course in the Winter 2005 Quarter. Dr. Hicks' guidance and the material studied in that course was invaluable to this research effort.

Finally, I would like to express my heartfelt appreciation to my wife and soul mate for her support during my time at AFIT and throughout my career. To her I owe thanks for helping me to maintain perspective and always focus on the important things in life. She is truly an unsung hero.

Charles A. Bilbey

Table of Contents

List of Figures

<div align="right">Page</div>

Page

List of Tables

INVESTIGATION OF THE PERFORMANCE
CHARACTERISTICS OF RE-ENTRY VEHICLES

I. Introduction

Background:

This study of Re-entry Vehicle (RV) systems and their associated operations was conducted in support of such agencies as the National Air and Space Intelligence Center. NASIC is the sole national center for integrated intelligence on aerospace systems, forces, and threats. They produce integrated, predictive air and space intelligence

Figure 1-1: Reentry vehicles from a recent Peacekeeper flight test streak into the Kwajalein target zone.

to enable military operations, force modernization and policymaking. NASIC has a long line of success stories that until recently could not be told outside of the Intelligence Community. NASIC products and services play a key role in assuring that American forces avoid technological surprise and can counter the foreign air and space threat (12).

The purpose of this study was to investigate and identify performance characteristics from re-entry to impact of an atmospheric re-entry vehicle. This includes re-entry vehicle

system background, description of re-entry systems, and mathematical simulation of performance characteristics.

We are at an early stage in the development of sound approaches, analytic tools and appropriate measures for assessing military competition in space, either today or in coming decades. In fact, we may not have even found the right metaphors and historical analogies for thinking about the military use of near-earth space. Today "the importance of the space mission to our national security cannot be overstated," Marine Gen. James E. Cartwright said in his April 4 testimony before the Strategic Forces subcommittee of the Senate Armed Services Committee (2:5). The United States is very dependant upon the use of space. Any threat to our ability to use it as desired deserves significant study. One such threat is through the use of a re-entry vehicle as a weapons delivery system.

The development of re-entry vehicles began in the late 1950's due to the need for Department of Defense and Central Intelligence Agency photo reconnaissance of Soviet ICBM sites. Film return capsules were used to retrieve photographs taken of intelligence targets on Earth from space. Part of a once-secret program known as Corona, the film "buckets" returned more than 800,000 images taken by Corona's KH-series cameras between August 1960 and May 1972, when the program ended (13:167-73) . The capsules and cameras were ejected by Corona's Agena spacecraft in orbit, reentered the atmosphere, and were retrieved in midair. During the Cold War, Corona photographs eased fears that the Soviet Union might be preparing a nuclear surprise attack. NASA has also been involved in the use of re-entry vehicles since the early 1960's, including manned space programs Mercury, Gemini and Apollo (13:167-173).

Atmospheric entry is the transition from the vacuum of space to the atmosphere of any planet or other celestial body. The term is not used for landing on bodies which have no atmosphere; e.g. the Moon. Atmospheric re-entry refers to the return to an atmosphere previously left for space. Often in this study the word "atmospheric" is dropped and the term re-entry is taken to mean atmospheric re-entry in context.

One way to classify re-entry vehicles is by their ballistic coefficients. Early U.S. ballistic re-entry vehicles had a low ballistic coefficient, or beta. The ballistic coefficient is a combination of weight, drag, and cross-section of a vehicle ($\beta = W/C_DS$). Figure 1-2 shows the Apollo 15 and the Gemini command modules to give the reader an idea of the vehicle shape and size as it relates to a ballistic coefficient.

Gemini spacecraft diagram			Apollo after splashdown. (NASA)		
Gemini spacecraft diagram (NASA)			Apollo after splashdown. (NASA)		
Dimensions			**Dimensions**		
Height:	18.6 ft	5.67 m	Height:	36.2 ft	3.47 m
Diameter:	10 ft	3.05 m	Diameter:	12.8 ft	3.9 m
Volume:	90 ft³	2.55 m³	Volume:	218 ft³	6.17 m³
Weights			**Weights**		
Reentry module:	4,372 lb	1,983 kg	Command module:	12,807 lb	5,809 kg
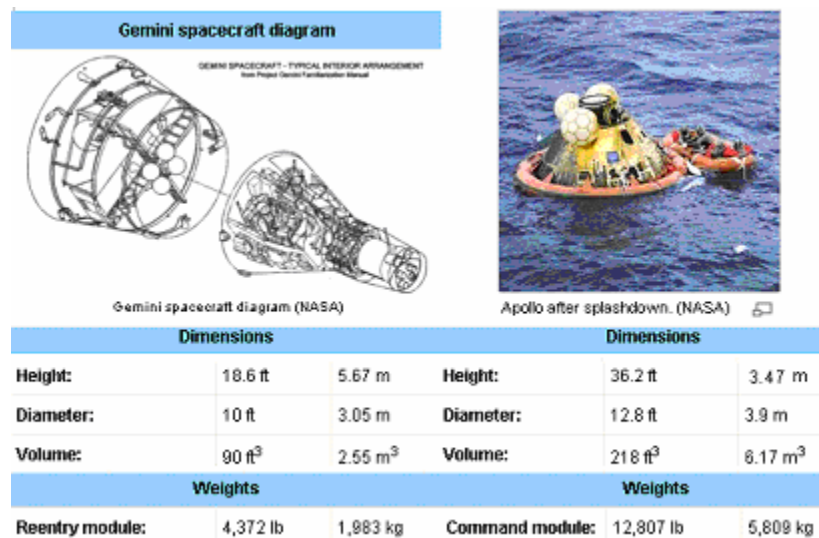
Fig 1-2: Re-entry Vehicle Dimensions

The drag coefficient (C_D) for the Gemini is .26 and for the Apollo it is .157. Using these values and the dimensions in Figure 1-2 the ballistic coefficients are calculated to be 1,472 kg/m² for the Apollo command module and 474 kg/m² for the Gemini module

3

(19:1;20:1) . For the purpose of this study our model vehicle will have a C_D of 1.3 and a ballistic coefficient of 1,827 kg/m^2.

Vehicles with a low beta do most of their slowing down in the thin upper atmosphere, above 120 km (7). They take longer to slow down and generate less heat, but experience this heat over a longer period of time. But missile designers wanted vehicles with a high beta, which are usually slender and smoother and generate less drag. They zip through the upper atmosphere without decelerating much and reach the ground still traveling very fast. This is desirable for missile re-entry vehicles (RVs) because the faster a warhead approaches its target, the harder it is for an enemy to shoot it down (7:1). Figure 1-3 is a graphical representation of the air density of the earth's atmosphere. As we will find in this study 80 km denotes the altitude at which the atmospheric density begins to effect the aerodynamics of the re-entry vehicle. An algorithm was developed in MATLAB to generate this plot and can be found in Appendix C.
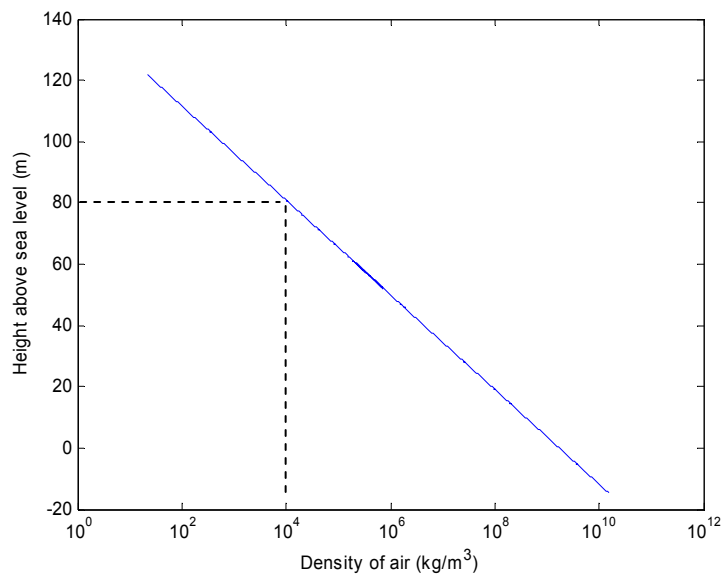
Fig: 1-3: Air Density of the Earth's Atmosphere

In 1968 the Boost Glide Re-entry Vehicle was a classified United States Air Force program to investigate missile maneuvering at hypersonic speeds after re-entry into the atmosphere. Upon re-entry, flight control was achieved by using aft trim flares and a reaction jet system commanded from an onboard inertial guidance system. It was launched from an Atlas missile booster and served to provide much data on hypersonic maneuvering flight characteristics. This data was of great value in developing later maneuvering re-entry vehicles. Upon re-entry into the earth's atmosphere, flight control was achieved through the use of the aft trim flares and a reaction jet system commanded from an on-board inertial guidance system instead of by aerodynamic controls (7:23). Figure 1-4 is a photograph of an actual Boost Glide Re-entry Vehicle (7:20).

Figure 1-4: The Boost Glide Re-entry Vehicle investigated related technological problems, particularly hypersonic maneuvering after re-entry into the atmosphere. The test was flown on 26 February 1968 from Vandenberg AFB, California to the area of Wake Island in the Pacific Ocean.

The evolving Soviet threat involved not just the development of ballistic missiles capable of intercontinental flight, but also the development of re-entry vehicles capable of

carrying nuclear warheads through the atmosphere to the target (the Soviets had also demonstrated fusion bomb technology in atmospheric tests). Furthermore, in the late 1960s and 1970s, Soviet missile systems became accurate enough to raise concern about their ability to destroy hardened targets in the United States, as did the Soviet deployment of large missiles capable of carrying multiple independently targeted re-entry vehicles. At the same time the Soviets were developing antiballistic missile systems, and in the mid-1960s actually deployed long-range interceptor batteries around Moscow together with the radars necessary to track re-entry vehicles at great ranges. It is this series of threats that the U.S. ballistic missile and re-entry system programs had to address (7:4).

In answering this threat, important improvements were made in areas such as guidance and control, command of missile systems in the field, and propulsion. Improvements to the missiles created opportunities for better re-entry systems, which was the focus of the Air Force's Advanced Ballistic Re-Entry Systems (ABRES) group (7:4). Initially, the objective of ABRES was to derive systems to penetrate Soviet antiballistic missile systems, which were undergoing significant testing and development at the time. U.S. intelligence indicated that the Soviets were developing a long-range exoatmospheric system based on an early-warning radar that would detect objects in its threat corridor and cue a second radar that tracked them with sufficient accuracy to launch a long-range interceptor. Defense penetration programs progressed in tandem with research and development of ballistic re-entry vehicles. The idea was to provide a number of options for neutralizing both current and anticipated Soviet antiballistic missile systems (7:5).

Today there are limited threats. But it's just a matter of time until the center of gravity of US military and commercial space will be challenged. We need to invest in methods for us to detect and understand when our systems are being threatened or attacked. A Military Utility Analysis (MUA) conducted during 1998 and 1999 showed the capabilities of a Space Maneuver Vehicle (SMV) would most likely be used for force enhancement, space control, and space test in the near future (15:9-10). Comparison of the SMV capabilities against the Air Force Space Command Strategic Master Plan (SMP) for 2000 showed the SMV to have a "direct and substantial" effect on 4 of the top 10 priorities in the near-term, and 6 of the top 10 priorities in the mid-term (15:11). When a non-US re-entry vehicle enters the earth's atmosphere, having the ability to accurately determine its performance profile is a primary concern.

Current technology being developed to demonstrate the feasibility of the SMV concept is the NASA and Boeing X-37. The Air Force is also contributing funds to the X-37 program to demonstrate technologies for future reusable military spacecraft. The X-37, shown in Figure 1-5, is being designed to operate on orbit as well as during the reentry phase of flight. The X-37 is capable of fitting into the Space Shuttle payload bay for launch into orbit, or it can be carried to orbit by an expendable launch vehicle (11:17).

A review of past research quickly led to a concentration on the operation of a maneuverable re-entry vehicle similar to the X-37. The "maneuverable re-entry vehicle" concept involves an RV capable of performing preplanned flight maneuvers during the re-entry phase. During a controlled re-entry, the vehicle's aerodynamic loads are maintained within acceptable limits by controlling the effect of lift and drag forces on the vehicle

Fig 1-5: X-37 Reusable Spaceplane (11)

throughout the flight. Maneuvering Reentry Vehicle (MaRV) concepts include both un-

powered and powered vehicles. Once a powered MaRV concept enters earth's atmosphere, a

propulsion system would be used to control descent and direct the RV to a landing site. For

the purposes of this study we will consider only the non-powered reentry case, using the

aerodynamic properties of the vehicle to evaluate its performance characteristics. Therefore,

the vehicle characteristics important to this study will be velocity, altitude, flight path angle,

lift to drag ratio, surface reference area, and vehicle mass. These characteristics will be used

to evaluate the profile or trajectory of the vehicle as it progresses through the earth's

atmosphere.

The goal of this study was to develop an algorithm capable of accurately

characterizing the profile of a maneuverable re-entry vehicle through atmospheric re-entry to

a final destination point on the ground. Predicting re-entry time and impact location relies on

observational data of the re-entry vehicle based upon the position and velocity of the orbital path and ideally from observations equally distributed over that path. For this reason we have chosen the known parameters of the X-37, a Space Maneuver Vehicle, to test the validity of the algorithm developed through this study.

This research begins by validating Vinh's classic first order solutions to the basic equations of planar entry trajectories. The plots generated will show how the changes to the lift-to-drag ratio affects the performance of the re-entry vehicle. Chapter II of this study will focus on setting up the re-entry problem. In Chapter II, we will validate the first order equations of motion governing a point-mass vehicle reentering the earth's atmosphere as developed by Vihn (17).

Chapter III will set up the atmospheric re-entry problem for the Re-entry Vehicle (RV) being modeled. First, the equations of motion for a point mass re-entering the earth's atmosphere will be stated. Next, the aerodynamic properties of the re-entry vehicle will be approximated and finally, assumptions will be made concerning the earth's atmosphere and gravitational field. Chapter IV will analyze the data by making lift-to-drag ratio changes at 400, 800 and 1200 seconds into the trajectory. In Chapter IV data from a published source document will also be run through the MATLAB$^{®}$ algorithm developed in this work and compared to the results generated by a FORTRAN algorithm developed in the source document. Chapter V will then summarizes the results and note recommendations for future areas of study. A general literature search that included the Office of Commercial Space Transportation's (OCST) data base, NASA, Air Force, and other technical libraries was performed.

II. The Re-entry Problem

Assumptions for Planar Entry Trajectories

Planar entry is defined as the motion confined to the plane of a great circle. Such a plane contains the vehicle's radius and velocity vectors and the earth's center point. The relevant geometry is depicted in Figure 2-1 and the 3-dimensional view in Figure 2-2. For the purpose of this study there is no consideration of flight controls to create a bank angle and therefore it is appropriate to consider planar entry.
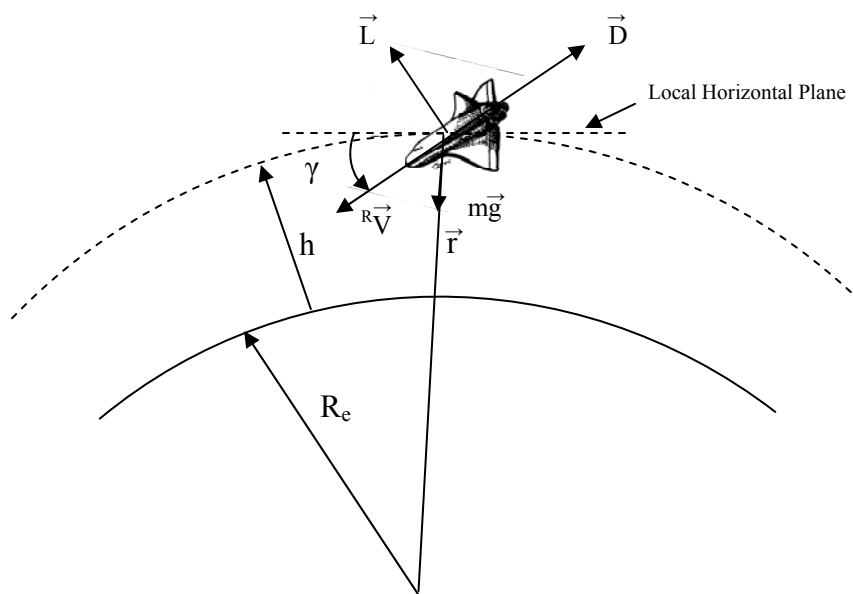
Fig. 2-1: Re-entry Coordinate System (14:101)
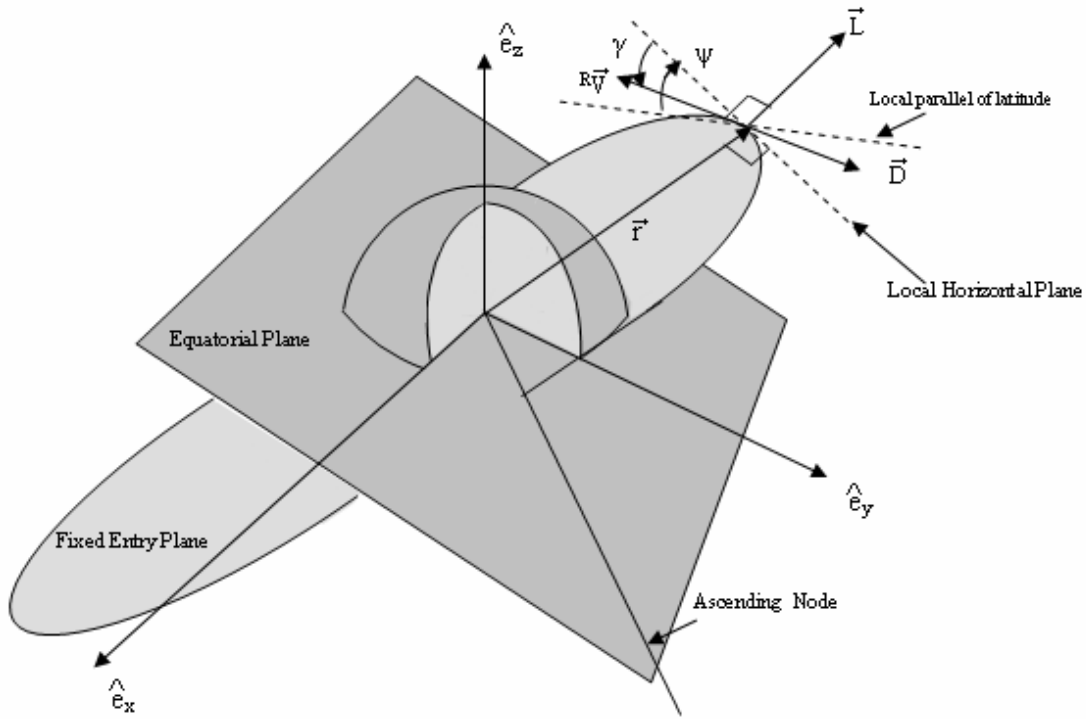
Fig. 2-2: Three-Dimensional View of Planar Entry (8:33)

Physical Assumptions

Along the entry trajectory the aerodynamic force plays an important role as a braking force to reduce the speed of the vehicle such that at the terminal phase of the flight the landing can be conducted as a vertical free fall using parachutes for a soft landing for a vehicle with no lift capability or as a gliding flight at low speed as an ordinary aircraft (17:100). The atmosphere is assumed to be strictly exponential, based on the surface density, ρ, and only a function of altitude (h). Thus, the atmosphere as a function of altitude is given by (14:38);

$$\rho = \rho_s * e^{-\beta h} \qquad (1)$$

where β^{-1} is a scaling height selected to best fit the atmosphere to the assumed exponential form. The parameters used to model the atmosphere for the purpose of this study are identified in Table 2-1.

Table 2-1: Atmospheric Re-entry Model Parameters (14:39)

Conditions	Value
Sea Level Density (ρ_s)	1.725 kg/km^3
Entry Altitude (h_0)	122 km
Earth's Radius (Re)	6378 km
Flight Path Angle at Entry	-.01 rad
Earth's Gravitational Parameter ($\mu=ge*Re^2$)	$3.99*10^5$ km^3/s^2
Distance of Vehicle from Center of Earth (r= Re + h_0)	6500 km
Acceleration of Gravity at Earth's Surface (ge)	$9.8*10^{-3}$ km/s^2

This atmospheric model is in agreement with the 1976 Standard Atmosphere to an altitude of approximately 120 km (14:29). The nonlinear differential equations which model the lifting re-entry vehicle are those for a unit point mass having lift and drag terms to represent the aerodynamic forces acting on the vehicle during re-entry given by (17:35);

$$D = \frac{1}{2} * \rho * C_D *^R v^2 * S \qquad (2)$$

$$L = \frac{1}{2} * \rho * C_L *^R v^2 * S \qquad (3)$$

where;

D = Drag (km/s^2)

L = Lift (km/s^2)

C_L = Lift coefficient

C_D = Drag coefficient

$$^Rv = \text{Earth-relative velocity (km/s)}$$

$$S = \text{Surface reference area}$$

The trajectory convention used for forces and angles are shown in Figure 2-1 (8:106).

Equations of Motion

The first step in examining a body re-entering the earth's atmosphere is to develop

a set of equations to describe the motion. If the RV is subjected to drag only, or ballistic

flight, the restriction of planar results in no loss of generality; however, if the RV is capable

of generating lift forces, then restricting it to a planar trajectory does limit the utility of the

result. Nevertheless, planar trajectory analysis can lead to closed-form expressions that can

be very useful in assessing re-entry vehicle performance. The coordinate system used is

constructed with one axis aligned with the earth relative velocity vector. The position of the

vehicle is defined by a vector from the center of the earth to the vehicle. Then, the plane

formed by this vector and the velocity vector is perpendicular to the second axis, with the

third axis completing the right-handed coordinate system (1:53). The motion of the vehicle

is measured by its velocity v and the flight path angle γ, between the velocity vector and the

local horizontal. The equations of motion developed in this coordinate system are (17:35):

$$\dot{r} = {}^Rv * \sin(\gamma) \tag{4}$$

$$^R\dot{v} = - \frac{D}{m} - g * \sin(\gamma) \tag{5}$$

$$^Rv\dot{\gamma} = - \frac{L}{m} - g * \cos(\gamma) + \frac{{}^Rv^2}{r} \cos(\gamma) \tag{6}$$

where:

$^\text{R}v$ = Earth-relative velocity (km/s)

g = Gravitational acceleration (km/s^2)

γ = Flight path angle (rad)

r = (Re + h) (km)

R$_e$ = Radius of earth (km)

h = Altitude of vehicle (km)

m = Mass of the vehicle (kg)

In this section there is no iteration, all equations have already been reduced and integrated by Vinh and will not be duplicated here (17). For the analysis of these first-order solutions, it is convenient to write the equations in non-dimensional form (17:48-54). Thus, the graphs developed are dimensionless and will merely show a trend relationship of the performance of one characteristic to another that is increasing or decreasing. A MATLAB® script was developed using the parameters in Table 2-1. The C_L/C_D ratios are representative of a minimum lift-to-drag ratio of .1 and maximum of 6.6 with three addition equal step sizes between the range determined by the algorithm and identified in Table 2-2.

Table 2-2: C_L/C_D Run Scenarios

RUN	C_L/C_D ratio
Run 1	.1
Run 2	1.725
Run 3	3.35
Run 4	4.975
Run 5	6.6

The derived parameters are given by (17:48-54):

$$\gamma = \frac{-2}{C_L/C_D * \beta * r_o} \left[\frac{\sqrt{g_o * r_o}}{v}\right]^2 \tag{7}$$

$$\beta r_0 \eta = \frac{\left(\frac{g_o * r_o}{v^2}\right) - 1}{C_L/C_D} \tag{8}$$

$$\frac{s}{r_o} = \frac{1}{2}\left[\frac{C_L}{C_D}\right] \ln\left(\frac{1 - \left(\frac{^R v}{\sqrt{g_o r_o}}\right)^2}{1 - \left(\frac{^R v_e}{\sqrt{g_o r_o}}\right)^2}\right) \tag{9}$$

$$\frac{a_{decel}}{g_o} = \frac{\left[1 - \left(\frac{^R v_e^2}{g_o * r_o}\right)\right]}{C_L/C_D} \tag{10}$$

where:

η is a non-dimensional altitude variable proportional to the density.

$^R v_e$ is the earth-relative velocity at entry.

C_L/C_D is the lift to drag ratio.

β is a scaling height selected to best match the atmosphere (.14 km^{-1}).

g_o is the acceleration of gravity at entry altitude.

r_o is the distance of the vehicle at entry from the earth's center.

s is the glide distance of the vehicle (range).

a_{decel} is the deceleration experienced during shallow, gliding entry.

The derivation of these equations is presented in *Hypersonic and Planetary Entry Flight Mechanics* and will not be duplicated in this writing (17:36-54). Certain assumptions have been employed to simplify the equations to the form presented above. Assuming a non-

rotating earth, and therefore a non-rotating atmosphere, in other words, the Coriolis and centripetal acceleration have been neglected. The Coriolis acceleration has an important effect in a high speed, long-range flight. For an accurate analysis of the problem of computing a trajectory for a ballistic missile this term should be included (17:27). However, for a first run analysis it will be ignored in this study. This assumption is appropriate since the effects of the rotating atmosphere on the vehicle are small compared to the aerodynamic forces due to the vehicle's velocity (14:3). This approach is also consistent with the equations used in *Shuttle Entry Guidance* (6:106).

Shallow Gliding Entry

At this point Equations (7) – (10) were coded in MATLAB$^{®}$ to examine the classic first order solutions to the basic equations of planar entry. This algorithm can be found in Appendix A. This step is important to demonstrate how altitude, speed, deceleration and other parameters interact during atmospheric entry. It is important to understand what should be expected of the trajectory for a lifting-body re-entry vehicle before considering the lifting re-entry problem in Chapter III. In Chapter III the equations of motion are not dimensionless and represent a specific vehicle model.

The first order analysis of a shallow gliding entry assumes the RV produces enough lift to maintain a lengthy hypersonic glide given a small flight path angle ($\gamma = -.01$ radians). Referring to Figure 2-1 the flight path angle (γ) is the angle formed between the vehicles velocity vector and the local horizontal plain. It can be thought of as describing how much the velocity vector contributes to moving "in and out" along the radius.

This allows the use of the small angle assumption where $\cos(\gamma) \approx 1$ and $\sin(\gamma) \approx \gamma$. This type of entry is an idealization; in reality it is not practical to maintain a small entry angle at hypersonic speeds all the way to the ground. However, it can be used to study large portions of the entry profile for a gliding entry. The Space Shuttle uses such an entry for its initial phase of re-entry, from entry interface to about 24 km in altitude (6:106).

Equations (7)-(10) were run through a MATLAB$^{\circledR}$ loop to create an array of data for each flight characteristic (i.e. $\gamma(n,m)$). In the array each column represents the values calculated with a given C_L/C_D at each increment of altitude, one column for each C_L/C_D run scenario. A circular orbit at the reference radius has a velocity of $\sqrt{g_{o*}r_o}$. If it is assumed this *reference velocity* is the maximum speed at which entry begins, then Figure 2-3 shows the altitude-velocity relationship in Equation (8) over the span of $0 < {}^Rv < \sqrt{g_{o*}r_o}$ for the various values of C_L/C_D. As altitude decreases η increases, the resulting range of $\beta r_0 \eta$ has not been limited to those that can be physically obtained. In Figure 2-3 we can see that if the C_L/C_D remains unchanged the flight path angle becomes steeper over the course of the glide.

Figure 2-4 shows the flight path angle-velocity relationship in Equation (7) for various C_L/C_D ratios, bearing in mind that the assumption of a small flight path angle begins to breakdown as the angle increases. As the flight path angle gets larger $\cos(\gamma)$ no longer equals one and the $\sin(\gamma)$ no longer equals γ.
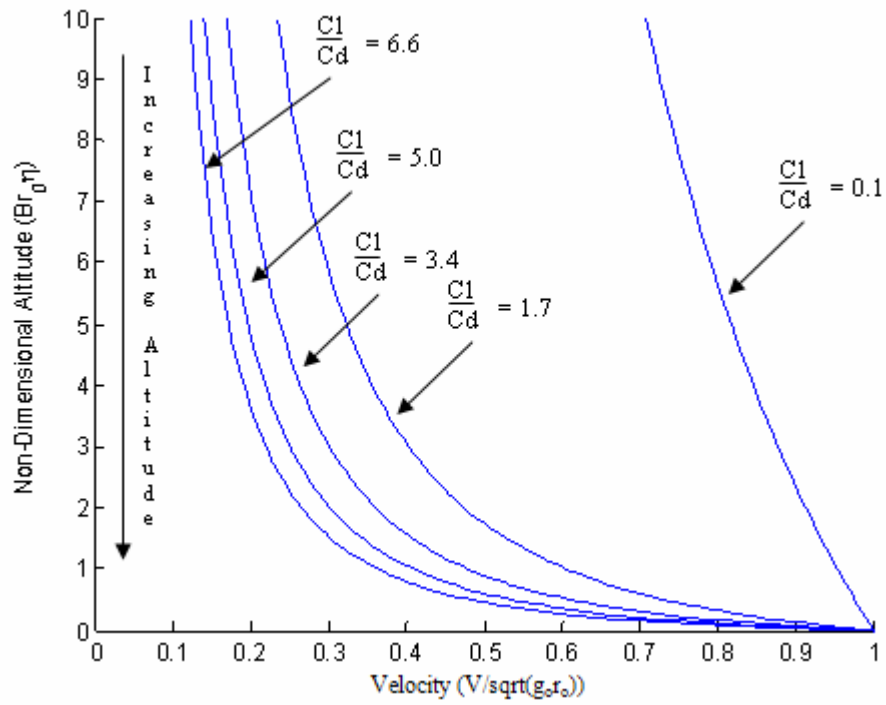
Fig 2-3: Velocity/Altitude Relationship
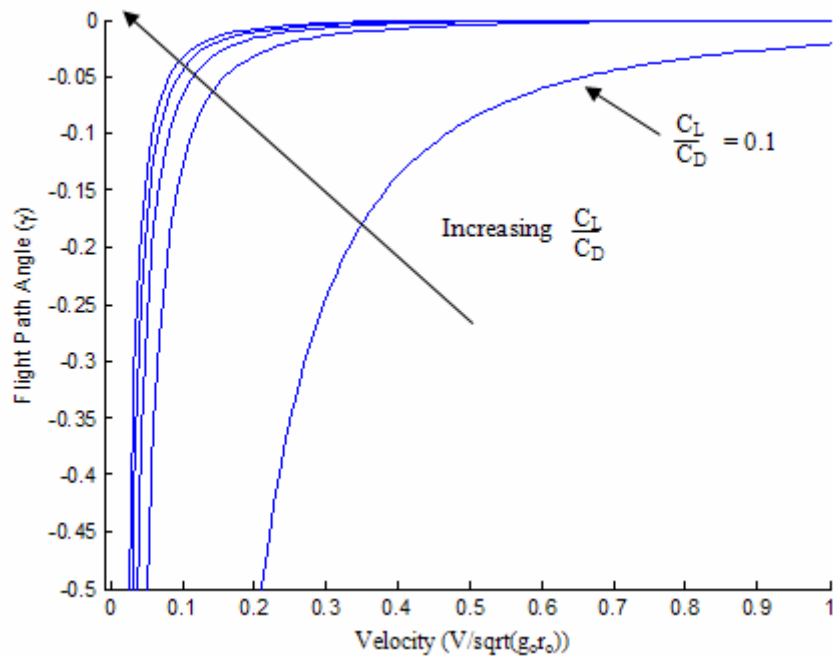
Fig 2-4: Velocity/Flight Path Angle Relationship

To determine the distance covered during the glide the expression for the velocity along the trajectory is given by integrating the arc-length from the entry velocity to the velocity relative to a particular instant in time to get the relationship expressed in Equation (9) and graphically displayed in Figure 2-5 (17:111). It is clear that the range can be maximized by using the largest lift-to-drag ratio available. An upper boundary on that limit can be found by artificially assuming the velocity can decrease to zero (17:111).
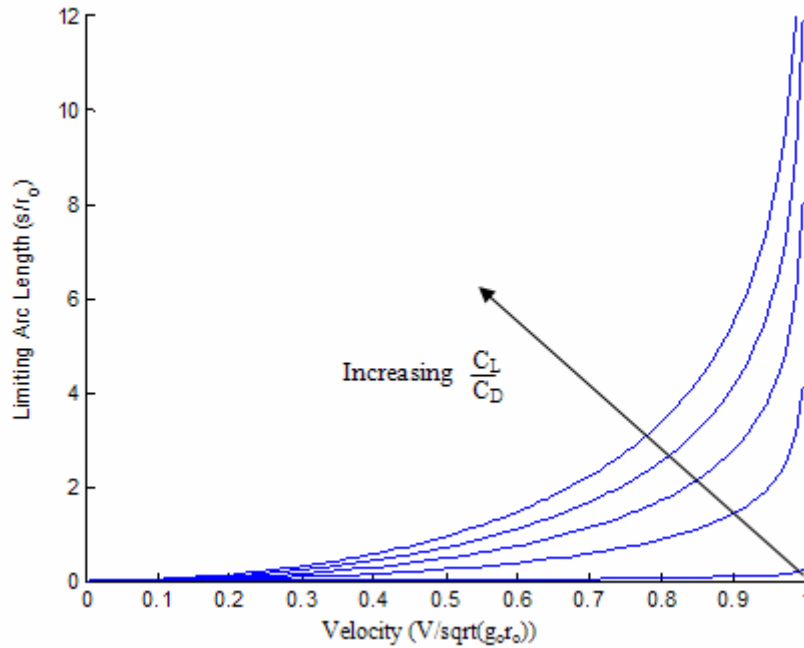
Fig 2-5: Max Glide Distance for Given Entry Speed

Similarly taking a final velocity of $^Rv = 0$ and integrating with respect to velocity yields a maximum flight time expressed by (17:112);

$$\sqrt{g_o/r_o}\ (t)_{limit} = \frac{1}{2}\left(\frac{C_L}{C_D}\right)\ \ln\left(\frac{1-\left(\frac{^Rv_e}{\sqrt{g_or_o}}\right)}{1+\left(\frac{^Rv_e}{\sqrt{g_or_o}}\right)}\right) \qquad (11)$$

As expected, Figure 2-6 shows that more lift results in more 'hang' time. For any prescribed speed the total time of flight is maximized by using the maximum lift-to-drag ratio.
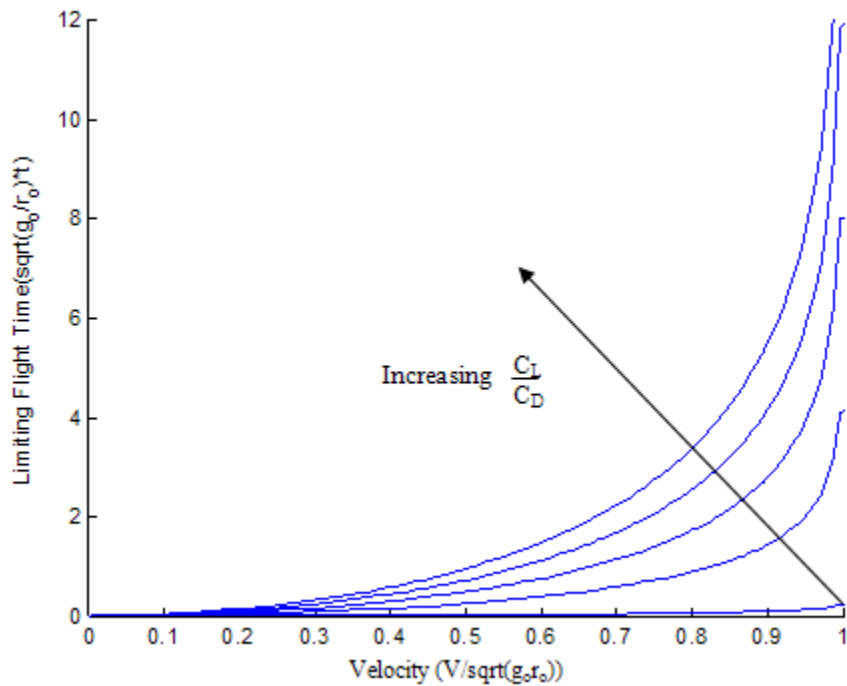
2-6: Max Glide Time for Given Entry Speed

Finally, while deceleration is more of a concern in developing a guidance algorithm and not a focus of this study, an expression for the deceleration experienced during a shallow, gliding entry can be expressed in terms of altitude and velocity by Equation (10) (17:113). Surprisingly Figure 2-7 shows that deceleration becomes larger as the vehicle slows and it continues to get larger throughout the trajectory. Equation (10) and Figure 2-7 also show that lift reduces the maximum deceleration. As the speed decreases, the deceleration increases continuously along the descending trajectory and it is minimized by using the maximum lift-to-drag ratio.
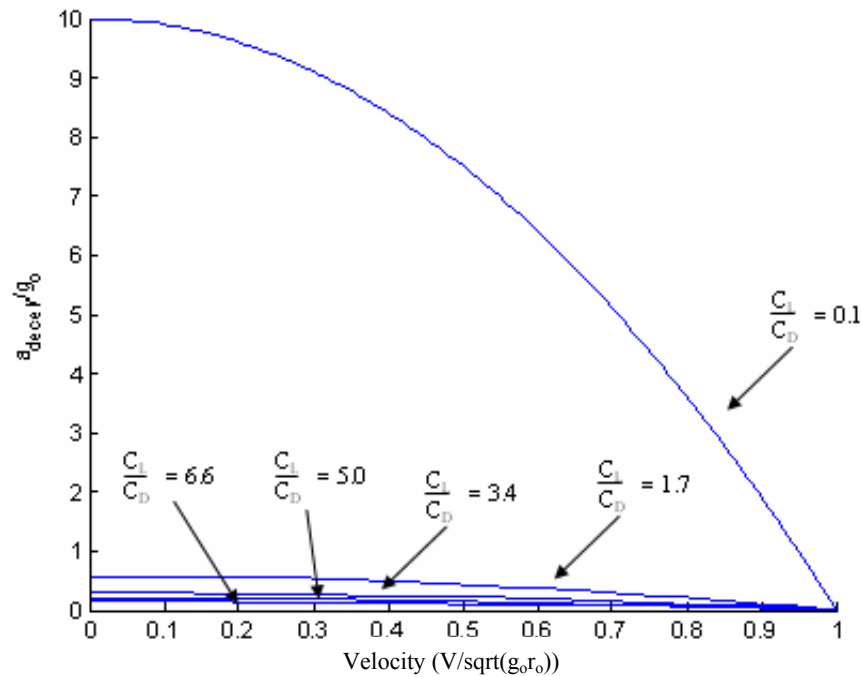
2-7: Velocity/a_{decel} Relationship

Summary

The equations and plots in this section have assisted in understanding the variations in altitude, speed, and the acceleration of the vehicle during entry into the earth's atmosphere. The first-order approximate solutions used in this chapter are designed for a specific and limited type of entry. The main assumption for this type of entry was a small flight path angle, which allowed the use of the small angle assumption where $\cos(\gamma) \approx 1$ and $\sin(\gamma) \approx \gamma$.

In examining the trajectory of the re-entry vehicle using the MATLAB® script it can be seen that the range can be maximized by using a larger lift-to-drag ratio and the speed decreases as the altitude decreases during the glide. It is shown that for any final speed the total time of flight is maximized by using the maximum lift-to-drag ratio.

One challenge with re-entry is deceleration from high orbital speeds. To avoid the

re-entry vehicle performing a meteor-style landing, it has to slow down. An obvious way of slowing down is through atmospheric friction and drag (i.e. using wind resistance). The key challenge with successful reentry then is to brake as much as possible while still in higher atmospheric layers and avoid plunging downwards too quickly. While deceleration is more of a concern in developing a guidance algorithm and not a focus of this study it was shown that the deceleration increases continuously along the descending trajectory and is minimized by using the maximum lift-to-drag ratio.

The plots help to identify the expected performance of the trajectories given the changes in parameters. We can now use this information to aid in understanding what to expect when analyzing the equations of motion in the subsequent chapters.

III. Lifting Re-entry Vehicle

Chapter II focused on the first-order approximate solutions for a specific and limited type of entry. This chapter will explore the re-entry problem being considered and the theory discussed will be applied. In this chapter we consider a re-entry vehicle that is capable of producing lift and how that lift might be used to shape the trajectory. The problem being considered is a medium C_L/C_D lifting re-entry vehicle. A general phenomenon in lifting entry at high speeds is what is called the quasi-equilibrium glide condition (QEGC). The range of flight conditions in which the QEGC is valid depends on the lifting capability of the vehicle. For vehicles with medium or higher lift-to-drag (L/D) ratios, such as the Shuttle, the range could cover the entire entry flight (7:23).

The atmosphere model used for this problem is the same model identified in Chapter II, Table 2-1. The atmospheric density will be expressed by (14:38);

$$\rho = \rho_s * e^{- h/H} \tag{12}$$

where the atmospheric scale height (H) is a measure of how rapidly the atmospheric density is changing with altitude (h). In the previous chapter for the classic first order equations β^{-1} was used to represent the scale height. In this chapter $H = \beta^{-1} = $ scale height.

The position of the vehicle will be measured by the down range distance, s, from the re-entry point and the altitude, h. The motion of the vehicle is measured by its velocity, v, and the flight path angle, γ. The initial state vector is therefore $x = [v_o\ \gamma_o\ \psi_o\ h_o\ s_o\ n_o\ e_o\ \theta_0\ \lambda_0]^T$. The system of differential equations for the re-entry problem is (17:27):

$$\dot{v} = - g_o * \sin(\gamma) - \frac{C_D S v^2 \rho^{-h/H}}{2m} \tag{13}$$

$$\dot{s} = v * \cos(\gamma) \tag{14}$$

$$\dot{h} = v * \sin(\gamma) \tag{15}$$

$$\dot{\gamma} = \frac{v}{r} * \cos(\gamma) - \frac{g_o}{v} * \cos(\gamma) + \frac{C_L S v \rho^{-h/H}}{2m} * \cos(\varphi) \tag{16}$$

$$\dot{\psi} = \frac{v}{r} * \sin(\psi) * \tan(\theta) - \frac{1}{\cos(\gamma)} * \frac{C_L S v \rho^{-h/H}}{2m} * \sin(\varphi) \tag{17}$$

$$\dot{n} = v * \cos(\gamma) * \cos(\psi) \tag{18}$$

$$\dot{e} = v * \cos(\gamma) * \sin(\psi) \tag{19}$$

$$\dot{\theta} = \frac{v}{r} * \cos(\gamma) * \cos(\psi) \tag{20}$$

$$\dot{\lambda} = \frac{v}{r * \cos(\theta)} * \cos(\gamma) * \sin(\psi) \tag{21}$$

where;

h_o = initial entry altitude

v_o = initial entry velocity

ψ_o = initial heading angle measured from north

s_o = 0; initial down range distance from entry point

n_o = 0; initial distance traveled toward north

e_o = 0; initial distance traveled toward east

θ_o = initial latitude

λ_o = initial longitude

These equations assume planar entry and a non-rotating earth.

Vehicle Model

The equations presented in the preceding section act to model the dynamics of atmospheric re-entry. The purpose of this study is to examine the dynamics of a particular

lifting-body reentry vehicle that enters the earth's atmosphere at approximately 122 km at an

entry velocity of 7.6 km/s and descends through a non-rotating atmosphere on a planar

trajectory using angle of attack, α, as the control variable.

In order to study the reentry characteristics of a given vehicle, an aerodynamic model

of the vehicle must be developed.   For this study the re-entry vehicle considered was

modeled using the vehicle characteristics of the X-37. At present, the Space Maneuver

Vehicle exists in concept only; however, the X-37 program is actively developing

technologies in support of its development (11:1). What does exist for the SMV are nominal

values for vehicle dimensions; i.e. weight, length, wingspan, etc. (11:2). Table 3-1 below

presents the dimensions of the SMV taken from the Boeing SMV concept.

Next, the initial conditions for the reentry trajectory must be determined. The

re-entry trajectory will begin at an altitude of 122 km—the same altitude used for Shuttle

entry guidance (6:99). The velocity at reentry will be dependent upon the altitude of the

vehicle orbit. For this study, the initial orbit of the vehicle will be assumed circular.

Table 3-1: SMV Parameters (11:2)

Parameter	Value
Weight	10000 lb
Length	29 ft
Wingspan	15 ft
Height	9.5 ft

Therefore the initial velocity for the RV to enter the atmosphere will be just below circular

velocity of $\sqrt{\mu/r_0}$ or 7.6 km/s.

The aerodynamic shape and configuration (ballistic or lifting) of a reentry vehicle determines the severity, duration, and flight path of reentry experienced by the vehicle. A MATLAB® algorithm was developed to generate a Graphic User Interface (GUI) to enable the user to enter the flight characteristics of the re-entry vehicle. This along with the algorithms that define the atmosphere and integrate Equations (13) – (21) can be found in Appendix B. A screen shot of the GUI menu generated by this algorithm is shown in Figure 3-1. Using these vehicle characteristics, Equations (13) – (21) are integrated using the MATLAB® function called ODE45. In this function the time step is set at 1 second.
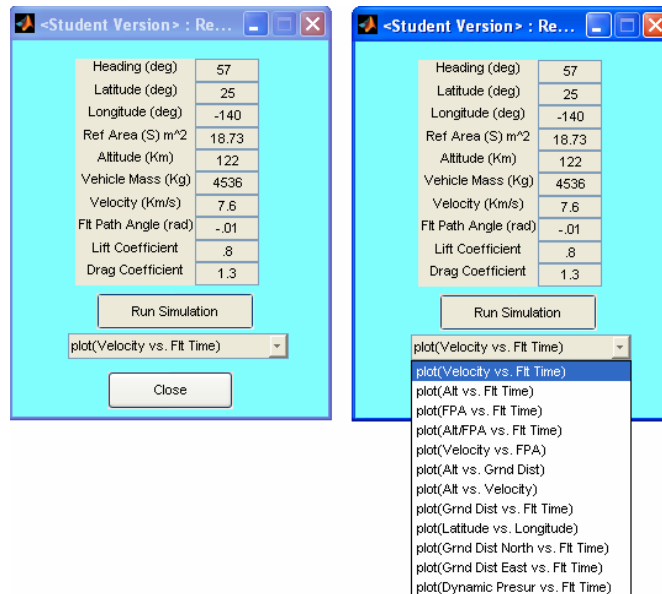
Fig 3-1: MATLAB® Graphic User Interface

Results

Once the simulation is run the user has the option to choose, from a drop down menu, to plot and examine different flight characteristics as they relate to flight time. Additional plots, not related to time, are available as well. Figure 3-2 is a plot of altitude vs ground

distance and shows the trajectory obtained by numerical integration of Equations (13) – (21)

when a non-maneuverable vehicle reenters at a velocity of 7.6 km/s and an entry flight path

angle (γ_0) of -.01 radians (-.57°) with a lift-to-drag ratio of .6. These initial conditions are

identified in Table 3-2.
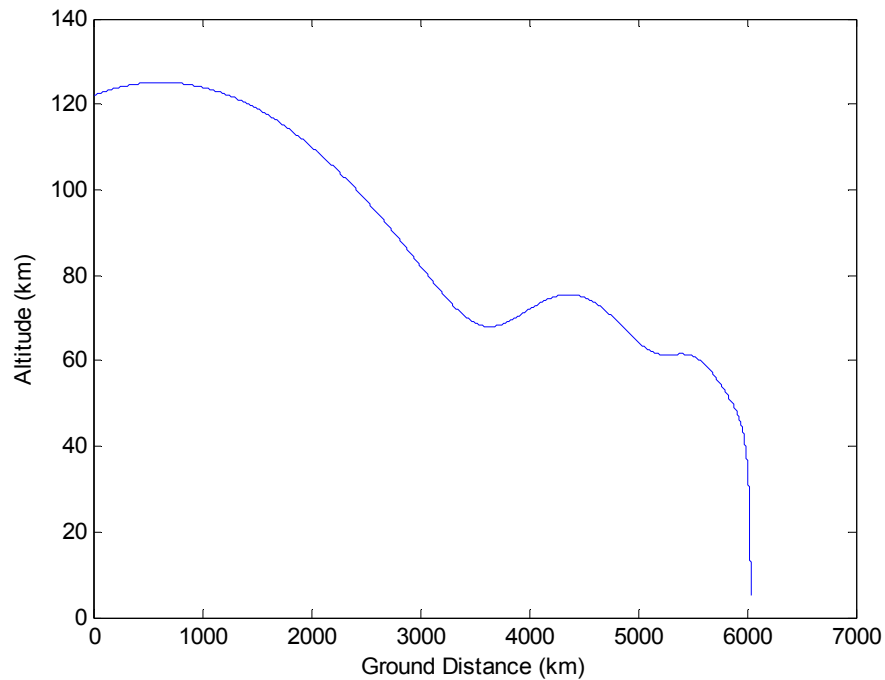
Fig 3-2: Altitude vs. Range

During a gliding re-entry, a vehicle such as the space shuttle creates enough lift to

maintain a long hypersonic glide at a small flight path angle. A measure of the vehicle's lift

that influences the descent path is the lift-to-drag ratio (4:242). For a given set of re-entry

conditions the motion of a lifting re-entry vehicle with a constant angle of attack is

determined by a vehicles actual lift and its lift-to-drag ratio. It should be noted that the more

gradual descents involve longer times and cover greater ranges than the steeper descents. For

example, starting at the same altitudes and velocities, a direct descent may traverse a distance

of only a few hundred miles and be accomplished in about 30 seconds; an orbital decay

might cover a range of a few thousand miles in 5 or 10 minutes; and a lifting descent might

extend over 5,000 to 10,000 miles in about 2 hours. A gradual descent involves a velocity

reduction and consequent energy dissipation over a long period of time (7:23).

Table 3-2: Initial Conditions for Re-entry (11:1)

Conditions	Value
Heading (ψ)	57°
Angle of Attack (α)	55°
Reference Area (S)	18.73 m^2
Altitude (h)	122 km
Vehicle Mass (m)	4536 kg
Velocity	7.6 km/s
Flight Path Angle (γ)	-.01 rad

The entry trajectory is divided into three phases:

    1. initial descent phase

    2. quasi-equilibrium glide phase

    3. terminal phase

As outlined by Figure 3-3, the initial descent is a *controlled fall* which takes the RV from the

entry interface at about 120 km in altitude to an altitude of about 80 km where the dynamic

pressure shown in Figure 3-4 has reached a sufficient level for aerodynamic lift to become

influential in shaping the trajectory depicted in Figure 3-3. While dynamic pressure loads are

more of a concern in developing a guidance algorithm and not a focus of this study Dynamic

pressure is an expression of velocity and atmospheric density given by;

$$q = \frac{1}{2} * v^2 * \rho^{-h/H} \tag{22}$$
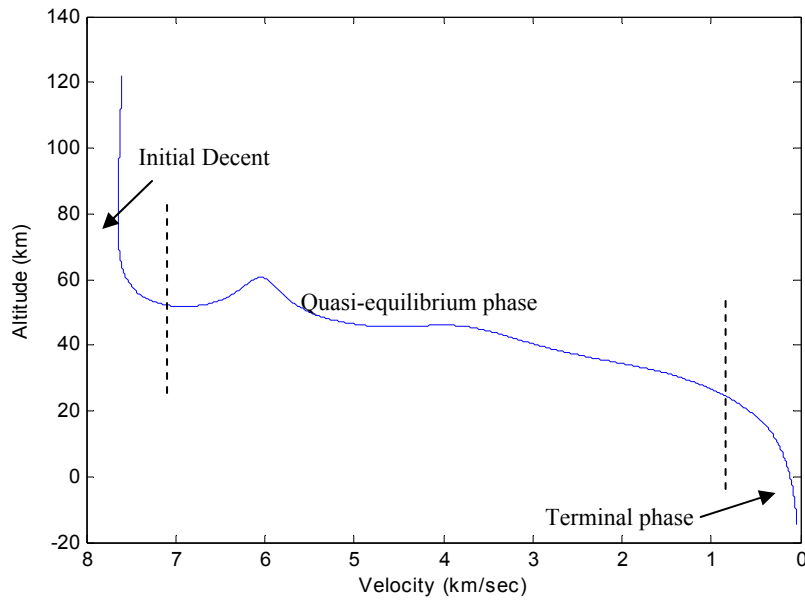
Fig 3-3: Altitude vs. Velocity
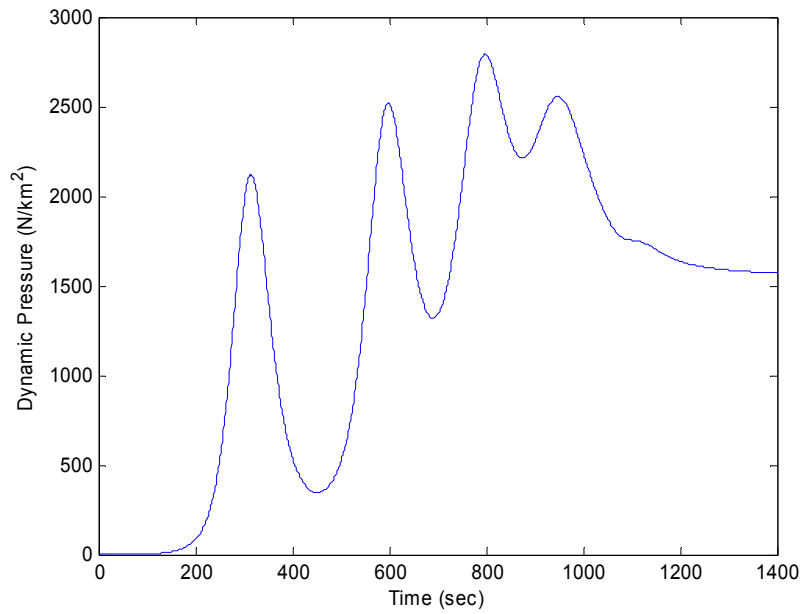
Fig 3-4: Dynamic Pressure vs. Time

The quasi-equilibrium glide phase covers the majority of the entry trajectory where all the path constraints must be observed and the range achieved must be correct for the RV to reach the landing site or impact point. In the terminal phase, the flight path angle as well as the altitude decreases rapidly. Once an altitude of approximately 80 km is reached, the velocity begins to decrease. At 20 km the velocity begins to decrease in a near linear manner.

Initial Descent Phase

Above 80–85 km in altitude, the Quasi-Equilibrium Glide Condition (QEGC) is not valid because the atmospheric density is too low. The path constraints are not a concern above that altitude for the same reason. Starting at the entry interface, the RV needs to descend and enter the entry flight corridor for the trajectory to transit smoothly onto a QEGC profile. This transition point marks the end of the initial descent phase. To determine the initial descent trajectory, the lift and drag coefficients are used to numerically integrate the equations of motion (13) – (21) with the given entry conditions.

Quasi-Equilibrium Glide Phase

It is well known in entry flight mechanics that in a major portion of a lifting entry trajectory, the flight path angle is small and varies relatively slowly. In this phase, the QEGC is valid, and the primary objectives in trajectory planning are to ensure observance of the path constraints and satisfaction of range requirement. The required range in the QEG phase is defined by Equation (13).

Figure 3-5 is a plot of the flight path angle, γ, versus velocity. The flight path angle at initial re-entry (γ_0) is - 0.57° (- 0.01 rads) and decreases to a minimum of - 58°. For the majority of the re-entry, the flight path angle remains between 0° and 2° (refer to Chapter IV, Figure 4-3). As the velocity decreases below 2 km/s the flight path angle begins to decrease rapidly, and the vehicle's rate of descent increases.
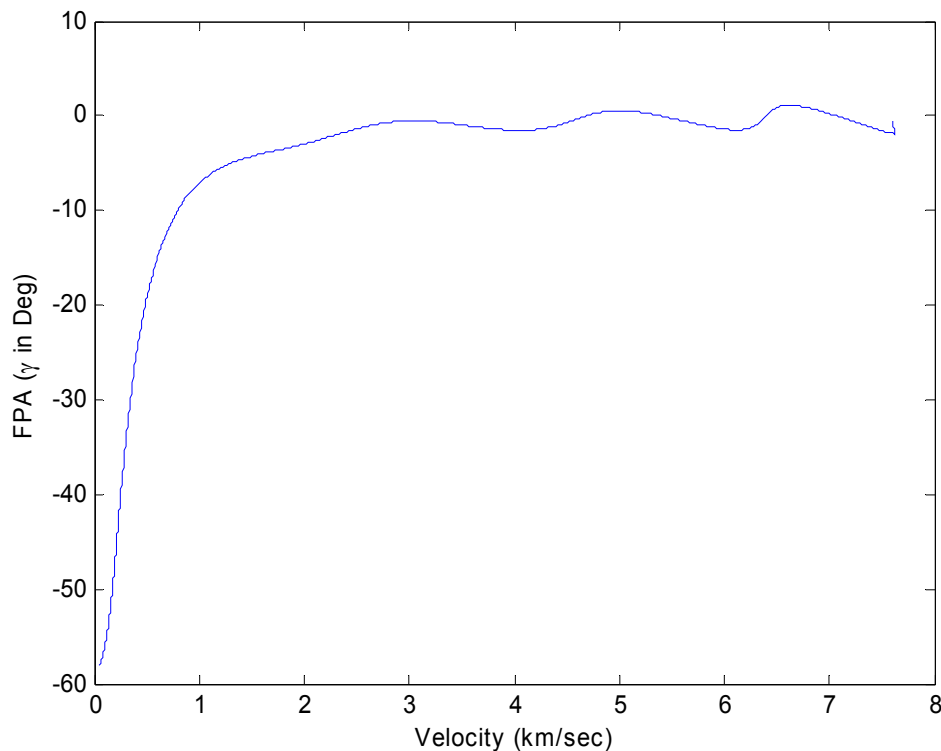
Fig 3-5: Flight Path Angle vs. Velocity

Terminal Phase

A change in velocity can be expected at the end of the QEG phase or start of the terminal phase. In this phase the flight path angle begins to decrease rapidly. If the trajectory planning in the preceding section extends to this phase, the obtained state profiles may not be flyable.

This Chapter applied the concepts of numerical integration to a non-maneuvering lifting re-entry problem with a constant lift-to-drag ratio. The developed algorithm produced a trajectory that describes the vehicle performance as it descends through the earth's atmosphere. The next logical step is to analyze the results.

IV. Comparison of Non-Maneuvering and Maneuvering Re-entry Vehicle

The primary goal of the algorithm employed in this study is to determine the flight characteristics of a re-entry vehicle as it progresses through the atmosphere to a termination point. In this chapter we compare a non-maneuverable re-entry vehicle with a constant .6 lift to drag (C_L/C_D) ratio to a maneuverable re-entry vehicle with a variable C_L/C_D ratio. A total of three maneuvers were performed in the maneuverable re-entry case. The C_L/C_D ratios for these maneuvers were found in a report on the optimal control of a space shuttle (3:8-9) and identified in Table 4-1.

Table 4-1: Lift-to-Drag Parameters (3:8-9)

Angle of Attack (α)	55°	20°	50°	55°
C_L	.8	.336	.655	.8
C_D	1.3	.244	.994	1.3
C_L/C_D	.6	1.38	.622	.6

As the amount of lift varies with the angle of attack, so too does the drag. Hence drag is the price we pay for lift. Thus, although it is desirable to obtain as much lift as possible from a wing, this cannot be done without increasing the drag. It is therefore necessary to find the best compromise. Table 4-2 identifies the changes in the C_L/C_D at the specified time intervals. The trajectory shown in figure 4-1 has an altitude at the bottom of the first dip of 68 km, which is reached after 400 seconds of flight. The approach taken for the analysis of the developed algorithm was to introduce a change to the lift-to-drag ratio (C_L/C_D) of the vehicle to simulate a maneuver that would level out the vehicle. The C_L/C_D was increased from .6 to 1.38 at 400 seconds into the trajectory where the dip at 68 km occurs. After

injecting the new C_L/C_D the vehicle experienced additional lift at 800 seconds at which time

the C_L/C_D was reduced to .622. Then at 1200 seconds the C_L/C_D was again reduced to .6 for

the remainder of the flight. Changes to the C_L/C_D were done in an effort to simulate a

possible maneuver that would be performed by a MaRV guidance system (3:8-9).

Table 4-2: Lift to Drag Ratio Change

Time	C_L/C_D
0 – 400	.600
400 – 800	1.38
800 – 1200	.622
1200 – end of flight	.600
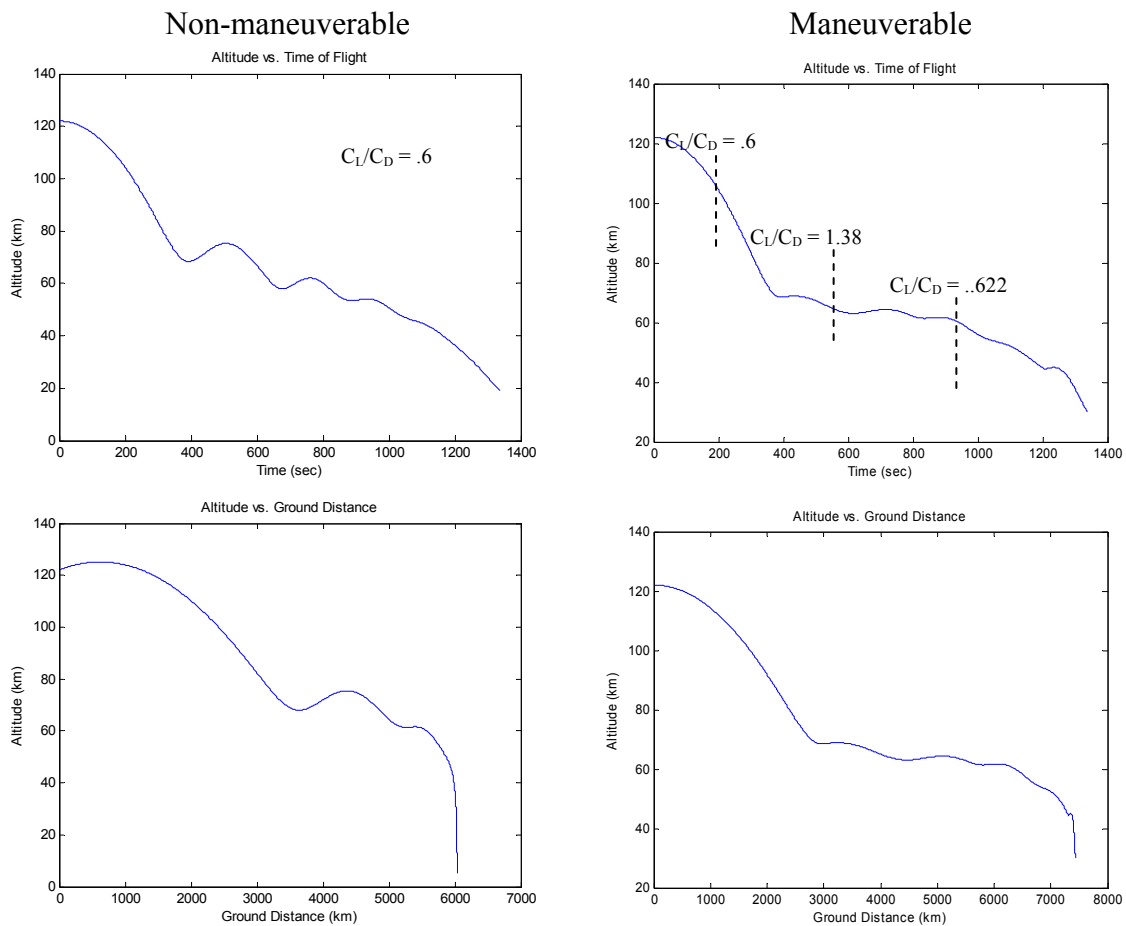
Fig 4-1: Analysis of Non-Maneuverable vs. Maneuverable Trajectory

The first maneuver was based on the vehicle's first encounter with the sensible

atmosphere at approximately 68 km. At this point an on-board guidance algorithm would

most likely perform a maneuver to level out the vehicle. Figure 4-1 also shows that lift

significantly increases the ground distance of the entry trajectory. It also shows that it is

easier to distinguish a maneuver higher in the less dense atmosphere. The second and third

maneuvers were performed at a point in the trajectory where additional atmospheric effects

were encountered and would most likely be countered with a maneuver. Maneuvers at lower

altitudes in the denser atmosphere were much less noticeable. An algorithm for the

automated change in C_L/C_D ratios can be found in Appendix B.

In Figure 4-2 it can be seen that once again the velocity remains essentially constant

until an altitude of approximately 80 km. Figure 4-3 shows the flight path angle as a function

of velocity. Again, for the majority of the re-entry, the flight path angle remains between 0°

and 2°.

Fig 4-2: Analysis of Altitude vs. Velocity

Non-maneuverable   Maneuverable
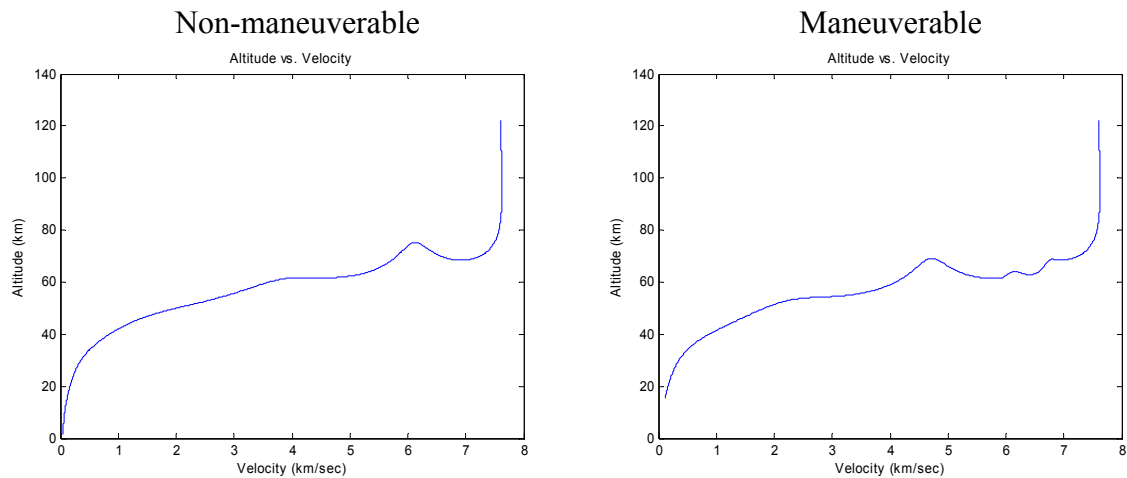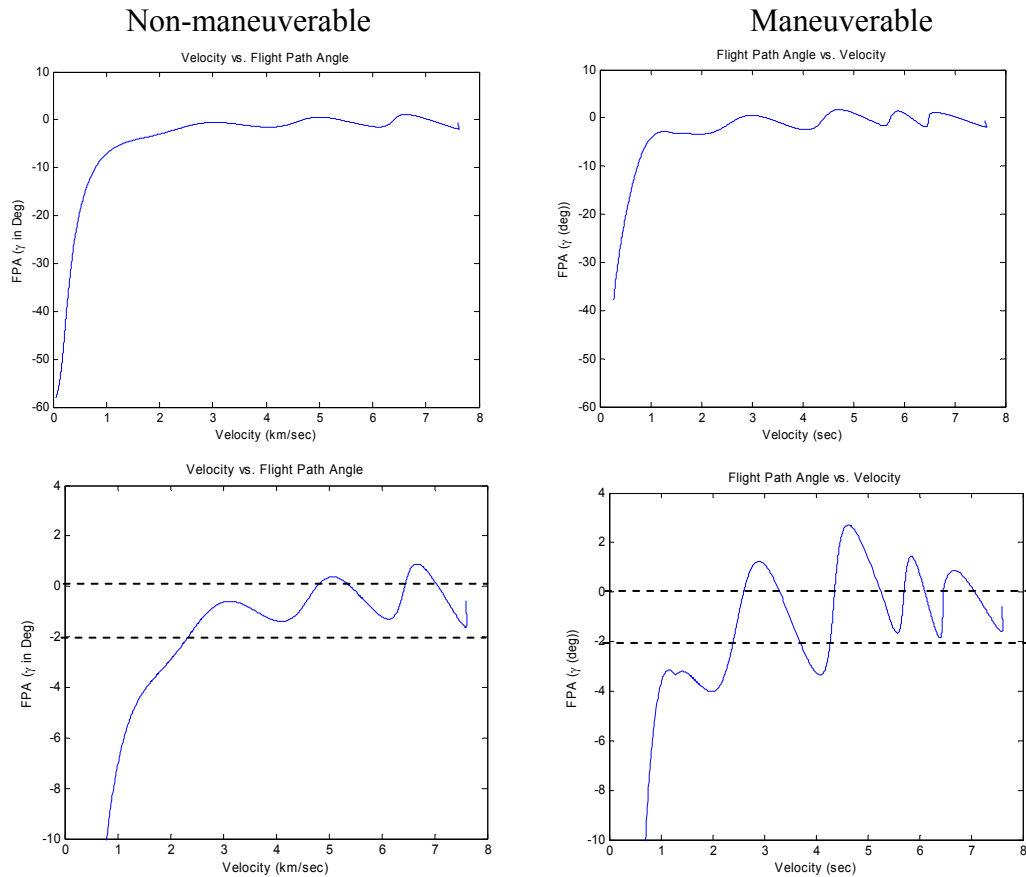
Fig 4-3: Analysis of Flight Path Angle vs. Velocity

Figure 4-4 shows the changes in velocity with each change to the lift-to-drag ratio.

As the vehicle maneuvers to maintain level flight the velocity does not decrease as quickly.

Figure 4-5 compares the altitude and flight path angle as they relate to time of the constant

C_L/C_D trajectory and the variable C_L/C_D trajectory. The MaRV maintains a small flight path

angle ($0 < \gamma < 2°$) for a much longer time. Figure 4-6 shows there is a slight increase of

dynamic pressure experienced by the MaRV due to atmospheric density.

Non-maneuverable   Maneuverable
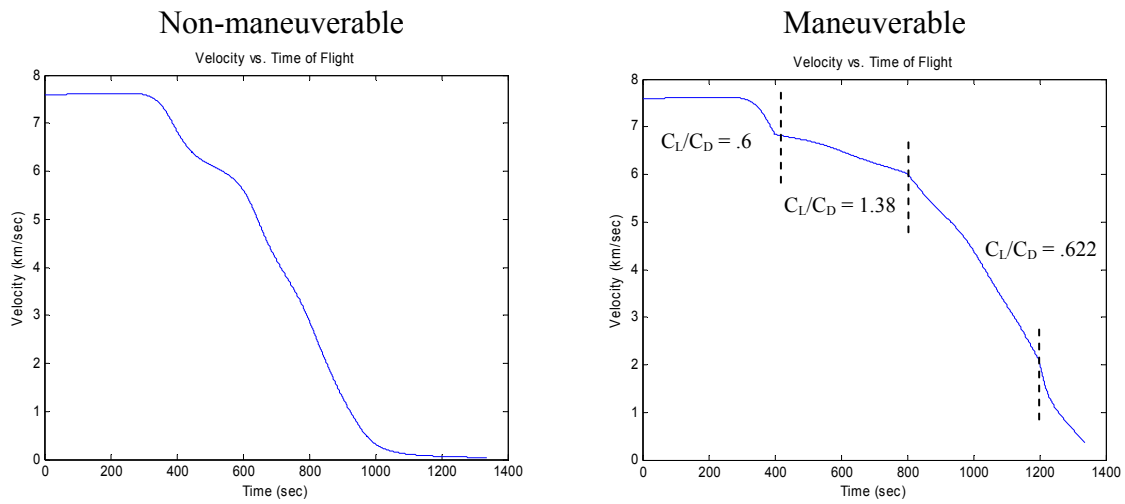
Fig 4-4: Analysis of Velocity vs. Time
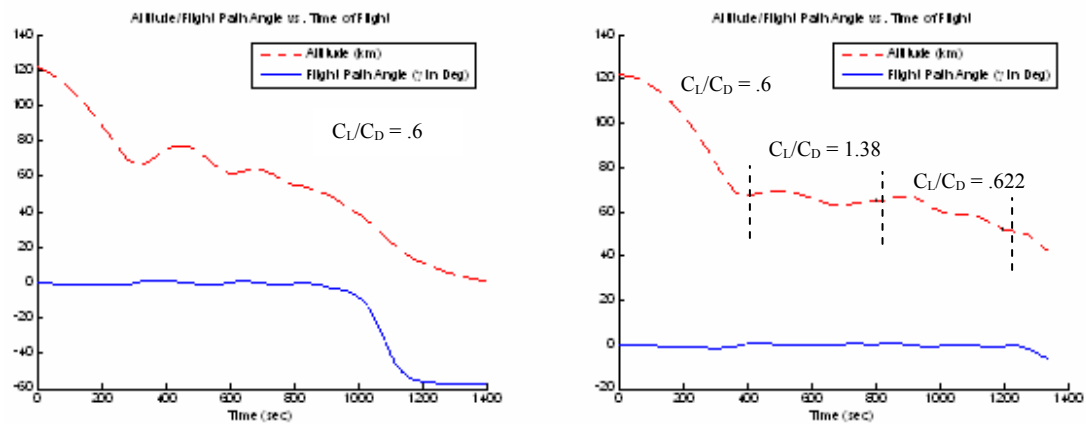
Fig 4-5: Alt/FPA vs. Time Analysis
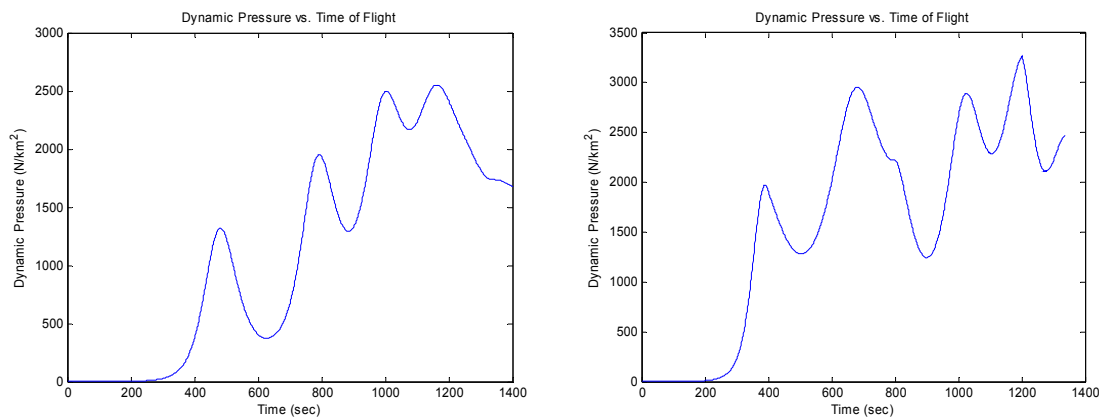
Fig 4-6: Dynamic Pressure Analysis

Validation

To test the validity of the developed algorithm an additional simulation was ran using data from a published source (9:4-2). The plots from the source document were then compared to the plots generated by the algorithm developed from this study. The initial conditions, as taken from the source document's output trajectory file are identified in Table 4-3 and the vehicle parameters are entered into the graphic user interface menu shown in Figure 4-7.

Table 4-3: Initial Entry Conditions (9:D-12)

Time (sec)	Alt (km)	Long (rad)	Lat (rad)	Vrel (km/sec)	FP (rad)	Heading (rad)
0.00000	393.2597	-1.878872	0.590298	18.22000	-1.221730	1.150579
0.02298	392.8659	-1.878872	0.590298	18.22019	-1.221713	1.150579
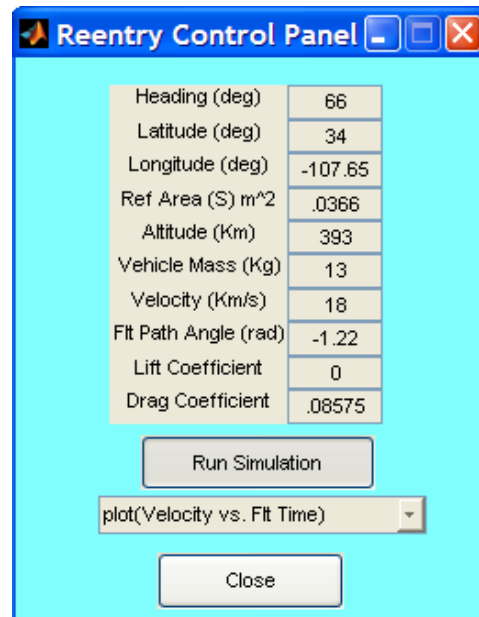
Fig 4-7: Graphic User Interface Menu

Figure 4-8 compares a plot of altitude vs. time generated by the MATLAB® algorithm developed in this study with the FORTRAN plot developed in a published source document

(9:4-2). The initial conditions and vehicle parameters from the source document were used to generate the MATLAB® plot. Both plots show an identical decline in altitude over time.
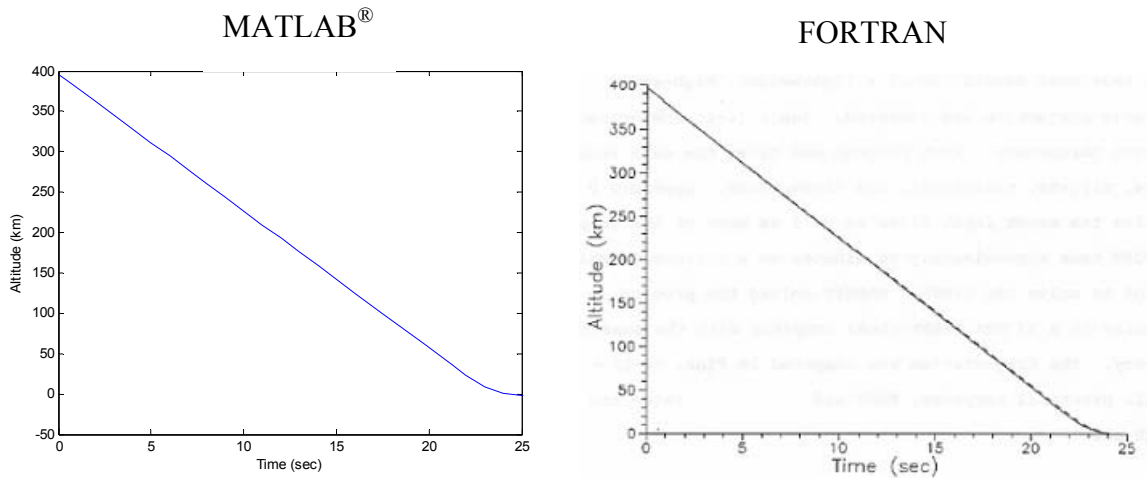
MATLAB®   FORTRAN

Fig 4-8: Altitude vs. Time Comparison

Figure 4-9 compares the MATLAB® plot of the vehicle's velocity with altitude and the source document's FORTRAN plot. Again the two plots identify a profile that is very similar. The intersecting dotted lines on the MATLAB® plot identify the lower boundary scale of the FORTRAN plot.

MATLAB®   FORTRAN
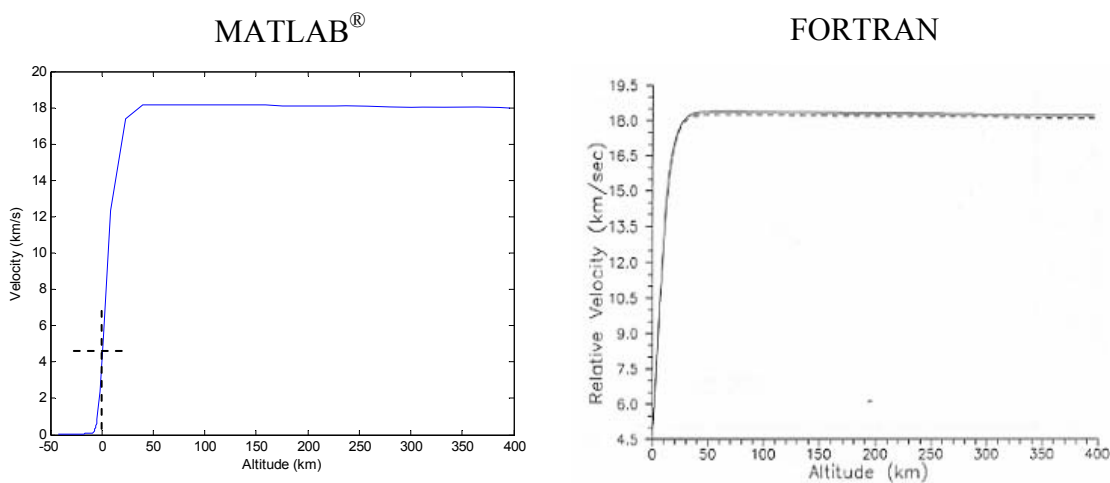
Fig 4-9: Velocity vs. Altitude Comparison

   Figure 4-10 compares plots of the flight path angle over time. For all practical

purposes both algorithms generated the same flight path with a 1% error.

MATLAB®   FORTRAN
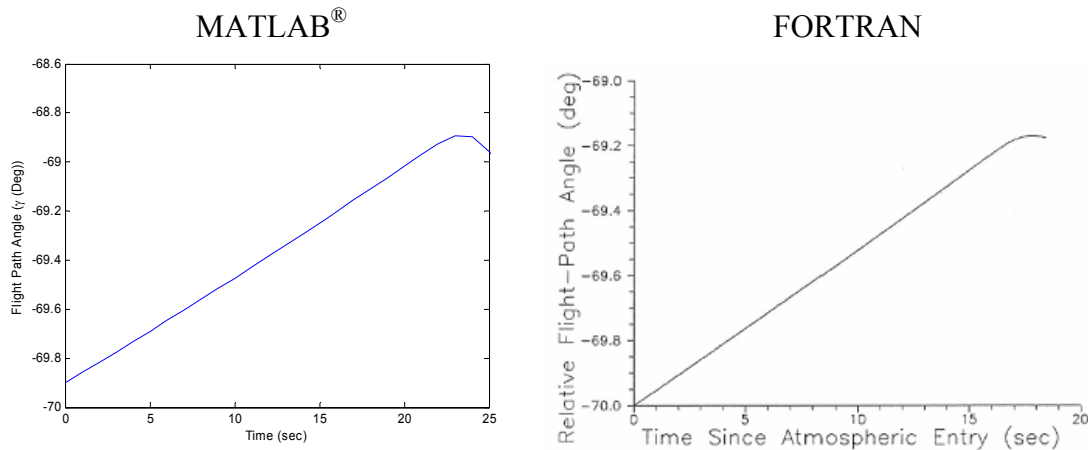
Fig 4-10: Flight Path Angle vs. Time Comparison

   Figure 4-11 is a comparison of plots showing the relationship between the vehicle's

velocity and flight time. It is evident that these comparisons further validate the accuracy of

the algorithm developed in this work. Differences can mainly be seen in flight time, which is

attributed to the rotation of the earth. The MATLAB® algorithm is based on a non-rotating

earth while the FORTRAN algorithm is based on a rotating earth.

MATLAB®   FORTRAN
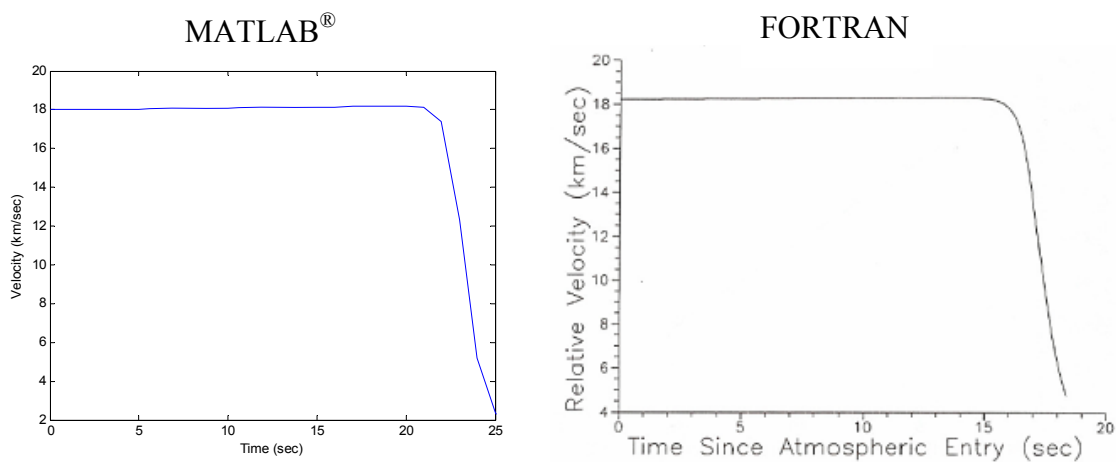
Fig 4-11: Velocity vs. Time Comparison

40

Analysis of Re-Entry Profile Prediction

The goal of this study was to develop an algorithm to determine the flight

characteristics of a re-entry vehicle—not to optimize the re-entry profile. The functionality

of the algorithm developed in this study is to allow the user to enter new flight characteristics

with each new maneuver of the MaRV. The initial analysis was run by changing the lift-to-

drag coefficient within an algorithm loop. The idea of this analysis was to use the Graphic

User Interface in Appendix C to enter the new flight characteristics as a result of the

maneuver at 400 seconds and 74.6 kms and plot the new trajectory. Then at 800 seconds and

55 kms perform a second maneuver entering the new flight characteristics again. The input

data for each of these post maneuver analysis was taken from the output trajectory file from

the initial run as explained in Appendix C. The plots are in agreement with the ones

generated using the method in the initial analysis.

Information from the results of the non-maneuvering RV was used to provide the data

for the maneuvers. At 400 seconds an altitude of 74.59 km was entered along with flight

path angle (γ) of -.0158 radians and using the same lift and drag coefficients as defined in

Chapter IV, Table 4-1. Figure 4-12 shows the two maneuvers as entered in the menu. This

data was taken from the trajectory output file (ydot) generated by the initial run and can be

found in Appendix B.

Figure 4-13 shows the two maneuvers as they relate to altitude as a function of time

and Figure 4-14 show how the altitude relates to the range. As expected when maneuvers are

made to maintain level flight the ground distance is greatly extended.

400 sec   800 sec
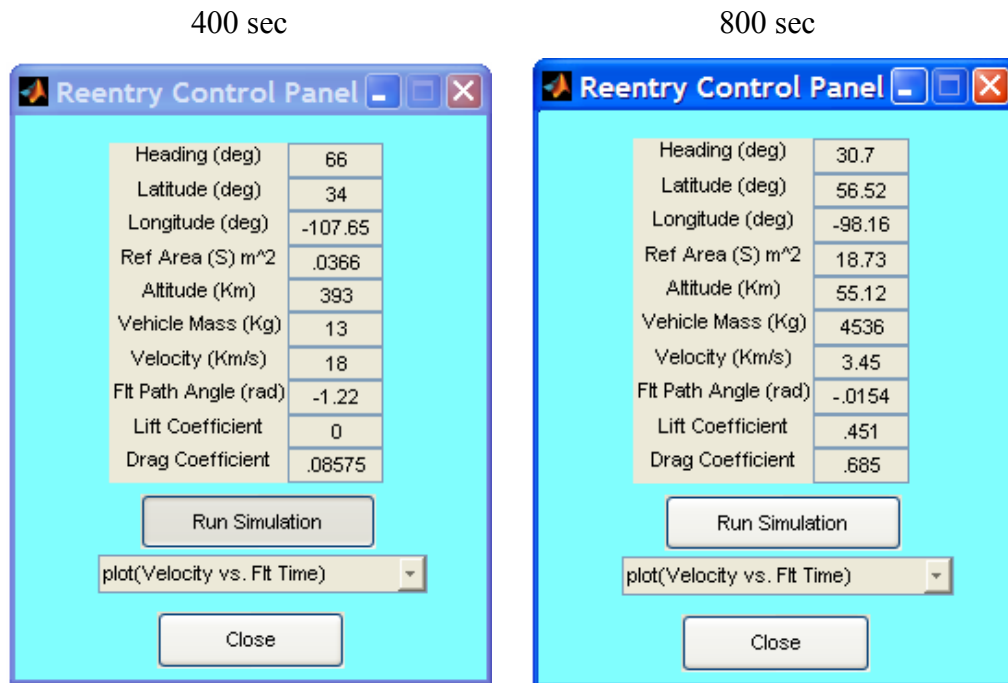
Fig. 4-12: Graphics User Interface menu

400 sec   800 sec
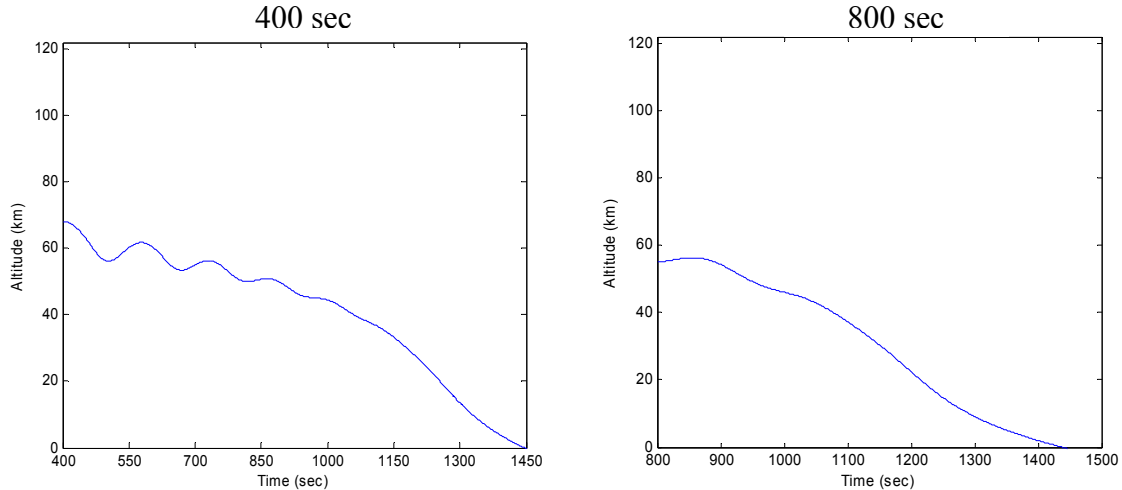
Fig. 4-13: Analysis of Altitude vs. Time

The total ground distance shown in right graph of Figure 4-14 agrees with the MaRV

analysis in the previous chapter.

400 sec

800 sec
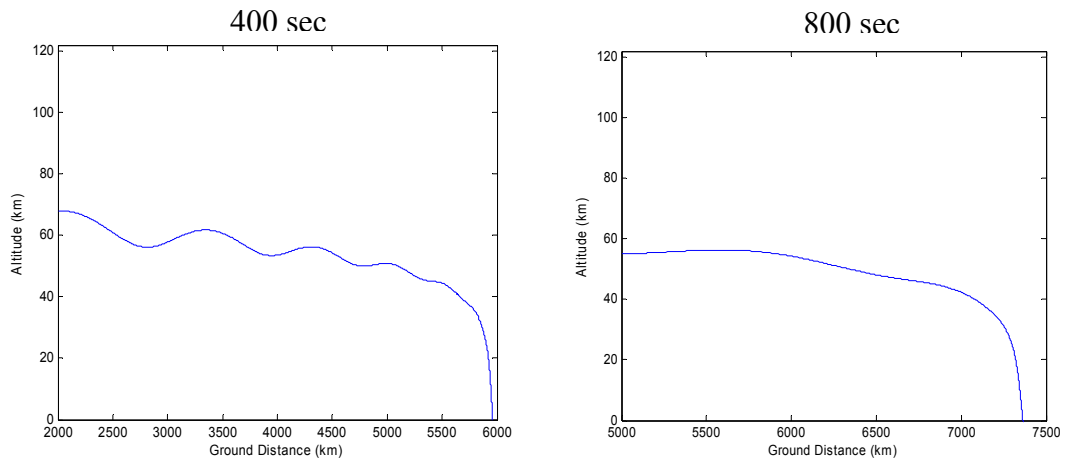
Fig. 4-14: Analysis of Altitude vs. Range

Figure 4-15 shows how the velocity relates to the flight time and Figure 4-16 shows the altitude as it relates to velocity. As the vehicle descends through the atmosphere it begins to slow due to the effects of the atmospheric density on the aerodynamic characteristics of the vehicle. This supports the results of the previous chapter.

400 sec

800 sec
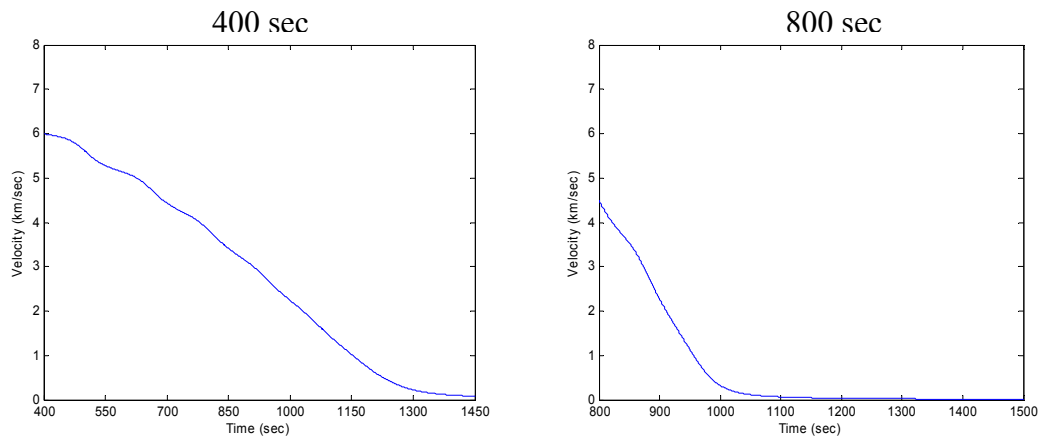
Fig. 4-15: Analysis of Velocity vs. Time
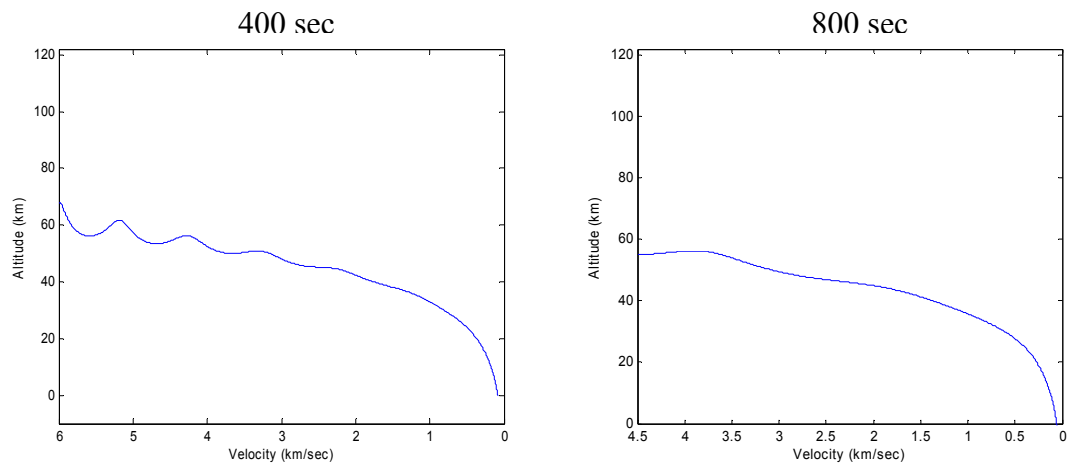
Fig. 4-16: Analysis of Altitude vs. Velocity

V. Conclusions and Recommendations

The objective of this study was to develop an algorithm that would accurately model the flight characteristics of a maneuverable re-entry vehicle through atmospheric re-entry to a termination point. Having done this, the following conclusions can be drawn from the analysis provided in Chapter IV.

1. The concept of modeling a re-entry trajectory using MATLAB software is an effective method for predicting the flight characteristics of an unknown vehicle entering the earth's atmosphere. It would be appropriate to say the studies involving maneuverable re-entry vehicles can be done starting at an altitude of 80 km.

2. Although the entry altitude was chosen to be 122 km, atmospheric effects are essentially negligible until the vehicle reaches an altitude near 80 km. Until 80 km altitude, the velocity and flight path angle remain essentially constant.

3. The maneuver at 74 km showed a greater effect on the trajectory. At least for the case studied, maneuvers performed higher in the less dense atmosphere appear to be more observable than those performed in the lower, denser atmosphere.

The following recommendations for further study are given:

1. The analysis conducted herein is somewhat limited by the assumptions made. Whereas this analysis could be used as an effective baseline, the fidelity of the simulation would have to be improved for an operational prediction method. In

particular, a more robust model of the earth's atmosphere accounting for cross-winds, hemispheric variations, and seasonal variations should be input into the guidance algorithm. The earth's rotation will need to be considered before any of these become important. Also, a higher order model of the earth's gravitational field, to include variation with altitude, as well as oblateness effects should be incorporated.

2. The vehicle parameters used are taken from the known parameters of the X-37 Space Maneuverable Vehicle. The parameters of mass, surface area and aerodynamics will require modification. Construction of a higher-fidelity model than the one used herein for use in determining the aerodynamic coefficients is one possible approach.

3. While the shuttle entry guidance is highly successful, search has been continued for entry guidance methods that enable fully autonomous and adaptive entry guidance. Currently the Shuttle's guidance algorithm is calculated on a known entry interface point and a known landing location. A key requirement for a system that allows full autonomous and adaptive entry guidance is to not rely on a reference trajectory generated on the ground. This study focused on the profile prediction method aimed at iteratively determining a trajectory leading from the current condition to the ground. This could be a first step in a fully autonomous and adaptive entry guidance system.

APPENDIX A

MATLAB CODE FOR FIRST ORDER ANALYSIS

Parameters

beta =..0.14 km^{-1}

earth radius =..6378 km

surface density =....................................1.217 kg/m^3

surface gravity =..................................0.00981 km/s^2

circular velosity =..................................7.8354 km/s

entry altitude =..122 km

radius at entry altitude =..........................6500 km

reference surface for lift/drag =..................18.7 m^2

mass of the vehicle =................................4536 kg

gravity at altitude =..........................0.0094452 km/s^2

Velosity at entry =..8 km/s

Flight Path angle at entry......................... -0.05 radians

eta at entry =..................................1.9542e-010 (non-dimensional)

$C_L/C_{D(1)}$ at entry...0.1 (non-dimensional)

$C_L/C_{D(2)}$ at entry.......................................1.725 (non-dimensional)

$C_L/C_{D(3)}$ at entry...3.35 (non-dimensional)

$C_L/C_{D(4)}$ at entry.......................................4.975 (non-dimensional)

$C_L/C_{D(5)}$ at entry...6.6 (non-dimensional)

Script to Define Parameters and Environment

```
%%%            First Order Equation verification
clc; clear all; close all
```

```
% ASSUMPTIONS:  Spherical, non-rotating Earth.
%               Constant Gravity
%               Exponential Atmosphere
%               Point mass re-entry vehicle


%%%%%%%%%%%%%%%%%%%%%%%%%%%%%%%%%%%%%%%%%%%%%%%%%%%%%%%%%%%%
% Parameters:
alt = 122;          %km
h = alt:-1:0;
vMIN = 0;
vMAX = 8;
vSTEP = length(h)-1;
v=linspace(vMAX,vMIN,vSTEP);
v_e = v(1);
gamma_e = -.05;
ClCdMIN = 0.1;
ClCdMAX = 6.6;
ClCdSTEP = 5;
ClCd=linspace(ClCdMIN,ClCdMAX,ClCdSTEP);
Cd=1
m = 8500;                           % kg - mass of vehicle
S = 10;                             % m^2 - reference surface for lift/drag
S_km = S/10^6;                      % km^2
beta = .14;                         % km^-1
rho_s = 1.217;                      % kg/m^3 - earth's density at surface
rho_s_km = rho_s*10^9;              % kg/km^3
r_earth = 6378;                     % km
gravity_s = 9.81e-3;                %km/sec^2
```

```
r_not = r_earth+alt;                    % km
g_not = (gravity_s) * (r_earth / r_not)^2;    % km/sec^2
mu = g_not*r_not^2;                     % km^3/s^2
v_c = sqrt(mu/r_not);                   % circular velocity
T = .5*(v_e/v_c).^2;                    % km^3/s^2
alpha=0:10:50;                          % Angle of Attack
Br0 = (beta * r_not);
eta_e =((rho_s*S*Cd)/(2*m*beta)) * exp(-beta * alt);    %Initialize counter


%%%%%%%%%%%%%%%%%%%%%%%%%%%%%%%%%%%%%%%%%%%%%%%%%%%%%%%%%%
% Call function to calculate re-entry characteristics
[eta, gamma, Br0n, Glide_Dist, Glide_Time, a_decel] = Shallow(v, v_e, h, S, m, Cd, eta_e,
Br0,  ClCd, beta, r_not, rho_s, g_not)
% Call function to plot re-entry performance
A = ShallowRngOutput(v, Br0n, gamma, ClCd, r_not, g_not, Glide_Dist, Glide_Time,
a_decel)
```

Function to Evaluate Equations of Motion

```
%%%%%%%%%%%%%%%%%%%%%%%%%%%%%%%%%%%%%%%%%%%%%%%%%%%%%%%%%%
function [eta, gamma, Br0n, Glide_Dist, Glide_Time, a_decel] = Shallow(v, v_e, h, S, m,
Cd, eta_e, Br0, ClCd, beta, r_not, rho_s, g_not)
% Shallow, gliding entry

eta =((rho_s*S*Cd)/(2*m*beta)) * exp(-beta * h);
%Initialize counter
p=1;
for m = 1:length(ClCd)              %counter #3, loops the # of lift/drag ratio values tested (5
times in this case)
```

```
    n=1;
    while n < (length(eta));
        %Build 2-dimensional matrices, where each column is the value
        %starting at entry altitude and going to h=0

        %Flight Path Angle, gamma
        gamma(n,p) = (-2/(ClCd(m)*Br0))*((sqrt(g_not*r_not)/v(n))^2);

        %Altitude with repect to eta
        Br0n(n,p) = (((g_not*r_not)/v(n)^2)-1)/ClCd(m);

        %Max Glide Distance
        Glide_Dist(n,p) = .5*ClCd(m)*log(1/(1-(v(n)/sqrt(g_not*r_not))^2));

        %Max Glide Time
        Glide_Time(n,p) = .5*ClCd(m)*log((1+(v(n)/sqrt(g_not*r_not)))/(1-
            (v(n)/sqrt(g_not*r_not))));

        %Deceleration
        a_decel(n,p) = (1-(v(n)^2/(g_not*r_not)))/ClCd(m);
        n=n+1;
    end
    p=p+1;
end
end
```

Output Function

```
% Plot re-entry performance
function A = ShallowRngOutput(v, Br0n, gamma, ClCd, r_not, g_not, Glide_Dist,
Glide_Time, a_decel)
```

```
A=(v/sqrt(g_not*r_not))'

figure(1)
xlabel('Velosity (V/sqrt(g_o/r_o)))')
ylabel('Altitude (Br_0\eta)')
title('Velosity/Altitude Relationship')
axis([0 1 0 10])
hold on
for i = 1:length(ClCd)
    plot(A(:,1), Br0n(:,i))
end

figure(2)
xlabel('Velosity (V/sqrt(g_o/r_o))')
ylabel('Flight Path Angle (\gamma)')
title('Velosity/FPA Relationship')
%axis([0 1 0 -.5])
hold on
for i = 1:length(ClCd)
    plot(A(:,1), gamma(:,i))
end
hold off
figure(3)
xlabel('Velosity (V/sqrt(g_o/r_o))')
ylabel('Limiting Arc Length (S/r_0)')
title('Max Glide Distance for Given Entry Speed')
axis([0 1 0 12])
hold on
for i= 1:length(ClCd)
    plot(A(:,1), Glide_Dist(:,i))
```

```
    end
hold off

figure(4)
xlabel('Velosity (V/sqrt(g_o/r_o))')
ylabel('Limiting Flight Time(sqrt(g_o/r_0)*t)')
title('Max Glide TIme for Given Entry Speed')
axis([0 1 0 12])
hold on
for i= 1:length(ClCd)
    plot(A(:,1), Glide_Dist(:,i))

end
hold off

figure(5)
xlabel('Velosity (V/sqrt(g_o/r_o))')
ylabel('a_d_e_c_e_l_//g_o')
title('Velosity/a_d_e_c_e_l Relationship')
axis([0 1 0 10])
hold on
for i= 1:length(ClCd)
    plot(A(:,1), a_decel(:,i))
end
hold off
end
```

APPENDIX B
ALGORITHM FOR RE-ENTRY TRAJECTORY

<u>Function to Generate Graphic User Interface</u>

```matlab
function reentrygui(varargin)

global A B C D E F G H N W L T t q y x pu
global Vnot ydot hnot m CL CD ClCd psiinit totalt rhoe rho AoA alpha alphanot psinot
gammanot

if nargin > 0, command = varargin{1}; end
if nargin >= 3, handles = varargin{3}; end
if nargin < 1

figure('color','b','units','normalized','position',[.6 .5 .2 .3],...
    'resize','off',...
    'menubar','None','name','Reentry Control Panel',...
    'numbertitle','Off','visible','on');

edit3 = uicontrol('Style','Edit','Units','Normalized',...
        'Position',[.58 .890 .2 .060],...
        'string',' ',...
        'Tag','Head',...
        'Visible','on',...
        'HorizontalAlignment', 'center');

edit4 = uicontrol('Style','Edit','Units','Normalized',...
```

```
            'Position',[.58 .830 .2 .060],...
            'string',' ',...
            'Tag','Lat',...
            'Visible','on',...
            'HorizontalAlignment', 'center');


edit5 = uicontrol('Style','Edit','Units','Normalized',...
            'Position',[.58 .770 .2 .060],...
            'string',' ',...
            'Tag','Long',...
            'Visible','on',...
            'HorizontalAlignment', 'center');


edit6 = uicontrol('Style','Edit','Units','Normalized',...
            'Position',[.58 .710 .2 .060],...
            'string',' ',...
            'Tag','Sref',...
            'Visible','on',...
            'HorizontalAlignment', 'center');


edit7 = uicontrol('Style','Edit','Units','Normalized',...
            'Position',[.58 .650 .2 .060],...
            'string',' ',...
            'Tag','Alt',...
            'Visible','on',...
            'HorizontalAlignment', 'center');


edit8 = uicontrol('Style','Edit','Units','Normalized',...
            'Position',[.58 .590 .2 .060],...
```

```
        'string',' ',...
        'Tag','Mass',...
        'Visible','on',...
        'HorizontalAlignment', 'center');


edit9 = uicontrol('Style','Edit','Units','Normalized',...
        'Position',[.58 .530 .2 .060],...
        'string',' ',...
        'Tag','Vel',...
        'Visible','on',...
        'HorizontalAlignment', 'center');


edit10 = uicontrol('Style','Edit','Units','Normalized',...
        'Position',[.58 .470 .2 .060],...
        'string',' ',...
        'Tag','FPA',...
        'Visible','on',...
        'HorizontalAlignment', 'center');


edit11 = uicontrol('Style','Edit','Units','Normalized',...
        'Position',[.58 .410 .2 .060],...
        'string',' ',...
        'Tag','Cl',...
        'Visible','on',...
        'HorizontalAlignment', 'center');


edit12 = uicontrol('Style','Edit','Units','Normalized',...
        'Position',[.58 .35 .2 .060],...
        'string',' ',...
```

```
            'Tag','Cd',...
            'Visible','on',...
            'HorizontalAlignment', 'center');


uicontrol('Style','text','Units','Normalized',...
            'Position',[.2  .890 .38 .060],...
            'String','Heading (deg)',...
            'Visible','on',...
            'HorizontalAlignment', 'center');


uicontrol('Style','text','Units','Normalized',...
            'Position',[.2  .830 .38 .060],...
            'String','Latitude (deg)',...
            'Visible','on',...
            'HorizontalAlignment', 'center');


uicontrol('Style','text','Units','Normalized',...
            'Position',[.2  .770 .38 .060],...
            'String','Longitude (deg)',...
            'Visible','on',...
            'HorizontalAlignment', 'center');


uicontrol('Style','text','Units','Normalized',...
            'Position',[.2 .710 .38 .060],...
            'String','Ref Area (S) m^2',...
            'Visible','on',...
            'HorizontalAlignment', 'center');


uicontrol('Style','text','Units','Normalized',...
```

```
'Position',[.2 .650 .38 .060],...
'String','Altitude (Km)',...
'Visible','on',...
'HorizontalAlignment', 'center');


uicontrol('Style','text','Units','Normalized',...
        'Position',[.2 .590 .38 .060],...
        'String','Vehicle Mass (Kg)',...
        'Visible','on',...
        'HorizontalAlignment', 'center');


uicontrol('Style','text','Units','Normalized',...
        'Position',[.2 .530 .38 .060],...
        'String','Velocity (Km/s)',...
        'Visible','on',...
        'HorizontalAlignment', 'center');


uicontrol('Style','text','Units','Normalized',...
        'Position',[.2 .470 .38 .060],...
        'String','Flt Path Angle (rad)',...
        'Visible','on',...
        'HorizontalAlignment', 'center');


uicontrol('Style','text','Units','Normalized',...
        'Position',[.2 .410 .38 .060],...
        'String','Lift Coefficient',...
        'Visible','on',...
        'HorizontalAlignment', 'center');
```

```
uicontrol('Style','text','Units','Normalized',...
        'Position',[.2 .35 .38 .060],...
        'String','Drag Coefficient',...
        'Visible','on',...
        'HorizontalAlignment', 'center');


T1=[...
    'plot(Velocity vs. Flt Time)            ';
    'plot(Alt vs. Flt Time)                 ';
    'plot(FPA vs. Flt Time)                 ';
    'plot(Alt/FPA vs. Flt Time)             ';
    'plot(Velocity vs. FPA)                 ';
    'plot(Alt vs. Grnd Dist)                ';
    'plot(Alt vs. Velocity)                 ';
    'plot(Grnd Dist vs. Flt Time)           ';
    'plot(Latitude vs. Longitude)           ';
    'plot(Grnd Dist North vs. Flt Time) ';
    'plot(Grnd Dist East vs. Flt Time)   ';
    'plot(Dynamic Presur vs. Flt Time) '];


run(1) = uicontrol('Style','togglebutton','Units','Normalized',...
        'Position',[.265 .23 .5 .1],...
        'String','Run Simulation',...
        'Visible','on',...
        'HorizontalAlignment', 'center',...
        'CallBack','reentrygui(1,gcbo,guihandles(get(gcbo,"Parent")))');


pu(2) = uicontrol('Style','Popup','Units','Normalized',...
        'Position',[.175 .12 .7 .1],...
```

```
            'String',T1,...
            'Visible','on',...
            'HorizontalAlignment', 'center',...
            'CallBack','reentrygui(2)');


uicontrol(...
        'CallBack','close all;',...
        'Units','normalized',...
        'Position',[.3 .02 .4 .1 ],...
        'String','Close',...
        'Style','pushbutton',...
        'UserData','');


return
end


if command == 1
    psiinitdeg = str2double(get(handles.Head,'string'));
    psiinit = psiinitdeg*(pi/180);
    hnot = str2double(get(handles.Alt,'string'));
    m = str2double(get(handles.Mass,'string'));
    Vnot = str2double(get(handles.Vel,'string'));
    gammanot = str2double(get(handles.FPA,'string'));
    Latinit = str2double(get(handles.Lat,'string'));
    Longinit = str2double(get(handles.Long,'string'));
    Sref = str2double(get(handles.Sref,'string'));
    CL = str2double(get(handles.Cl,'string'));
    CD = str2double(get(handles.Cd,'string'));
    ClCd = CL/CD;
```

```matlab
    Reentry
end

if command == 2
  switch get(gcbo,'value')
  case 1
    % Plot of Velocity vs. Time of Flight
      figure(2),clf, plot(t,A)
      xlabel('Time (sec)')
      ylabel('Velocity (km/sec)')
      title('Velocity vs. Time of Flight')
  case 2
    % Plot of Altitude vs. Time of Flight
      figure(3),clf, plot(t,D)
      xlabel('Time (sec)')
      ylabel('Altitude (km)')
      title('Altitude vs. Time of Flight')
  case 3
    % Plot of Flight Path Angle vs. Time of Flight
      figure(4),clf,
      plot(t,B*180/pi,'b')
      xlabel('Time (sec)')
      ylabel('\gamma (Deg)')
      title('Flight Path Angle vs. Time of Flight')
  case 4
    % Plot of Altitude and Flight Path Angle vs. Time of Flight
      figure(5),clf,
      hold on
      plot(t,D,'r')
```

```
        plot(t,B*180/pi,'b')
        hold off
        legend('Altitude (km)','Flight Path Angle (\gamma in Deg)')
        xlabel('Time (sec)')
        title('Altitude/Flight Path Angle vs. Time of Flight')
    case 5
      % Plot of Velocity vs. Flight Path Angle
        figure(6),clf, plot(A,B*180/pi)
        xlabel('Velocity (km/sec)')
        ylabel('FPA (\gamma in Deg)')
        title('Velocity vs. Flight Path Angle')
    case 6
       %Plot of Altitude vs. Ground Distance
        figure(7),clf, plot(E,D)
        xlabel('Ground Distance (km)')
        ylabel('Altitude (km)')
        title('Altitude vs. Ground Distance')
    case 7
      % Plot of Altitude vs. Velocity
        figure(8),clf, plot(A,D)
        xlabel('Velocity (km/sec)')
        ylabel('Altitude (km)')
        title('Altitude vs. Velocity')
    case 8
      % Plot Ground Distance vs. Time of Flight
        figure(9),clf, plot(t,E)
        xlabel('Time (sec)')
        ylabel('Ground Distance (km)')
        title('Ground Distance vs. Time of Flight')
```

```matlab
    case 9
      % Plot of Latitude vs. Longitude
        figure(10),clf, plot(L,T)
        xlabel('Longitude (degrees)')
        ylabel('Latitude (degress)')
        %title('Latitude vs. Longitude')
    case 10
      % Plot North Ground Distance vs. Time of Flight
        figure(11),clf, plot(t,F)
        xlabel('Time (sec)')
        ylabel('Ground Distance North (km)')
        title('Ground Distance North vs. Time of Flight')
    case 11
      % Plot East Ground Distance vs. Time of Flight
        figure(12),clf, plot(t,G)
        xlabel('Time (sec)')
        ylabel('Ground Distance East(km)')
        title('Ground Distance East vs. Time of Flight')
    case 12


%%%%%%%%%%%%%%%%%%%%%%%%%%%%%%%%%%%%%%%%%%%%%%%%%%%%%%%
    % BEGIN SECTION for calculating and plotting Dynamic Pressure(q)
    % Multiply by (1 km/ 1000m) to get units of N/m^2
    for i=1:totalt
      q(i,1)=(1/1000)*(0.5*((y(i,1))^2)*rhoe*exp(-y(i,4)/H));
    end
    figure(13),clf, plot(t,q)
    xlabel('Time (sec)')
    ylabel('Dynamic Pressure (N/km^2)')
```

```matlab
    title('Dynamic Pressure vs. Time of Flight')
    %%%END SECTION for calculating and plotting Dynamic Pressure(q)
  end
end
```

Script to Define Parameters and Environment

```matlab
%%%                         Re-Entry
%clear all; close all
% Program to calculate and plot 3-D atmospheric re-entry
% ASSUMPTIONS:  Spherical, non-rotating Earth.
%           Constant Gravity
%           Exponential Atmosphere
%           Point mass re-entry vehicle
global m Re ge S CD CL CLCD ClCd beta beta_m H ge rhoe rho phi tstep
global Vnot ydot hnot totalt rohe AoA alpha alphanot psinot gammanot
global A B C D E F G H N W L T t y

%%%%%%%%%%%%%%%%%%%%%%%%%%%%%%%%%%%%%%%%%%%%%%%%%%%%%%%%%%%%%%%
%Times
tstep=1;              % sec
tfinal=1400;          % sec
phi=0;               % Initial roll angle
index=0;             % Count variable


%%%%%%%%%%%%%%%%%%%%%%%%%%%%%%%%%%%%%%%%%%%%%%%%%%%%%%%%%%%%%%%
%Parameters
mu=3.99*10^5;         % Earth gravitational parameter (km^3/s^2)
Re=6378;              % Radius of the Earth in km
ge=9.81*10^-3;        % Constant gravity in km/s^2
```

```
S=Sref*10^-6;          % Reference Area km^2
rhoe=1.752*10^9;        % Surface density (kg/km^3)
H=6.7;                  % Scale Height in km
NZmax = 2.5 * ge;       % Maximum Normal Load (expressed in g's) (km/s^2)


% Heat constraint parameters
Cq=1.65*10^2;            % Heat Transfer Coefficient (w/m^2)
vref = .001;             % Reference Velocity (km/s)
rhoref=1*10^9;           % Reference Density (kg/Km^3)
qdotmax=5.443*10^11;    % Reference density for use in Max heating rate constraint
(kg/km^3)


%%%%%%%%%%%%%%%%%%%%%%%%%%%%%%%%%%%%%%%%%%%%%%%%%%%%%%%
% Dynamic Pressure Parameters
qmax = 1.628*10^10;                % Max allowable dynamic pressure 342 lb/ft^2
                                      converted to (N/km^2)


%%%%%%%%%%%%%%%%%%%%%%%%%%%%%%%%%%%%%%%%%%%%%%%%%%%%%%%
% Angle of Attack Profile
  alphaint=alphanot;
  alphafinal=20;
  Valpha1 = 20000*(3.0547e-4); % Velocity where angle of attack modulation begins (km/s)
  Valpha2 = Valpha1;            % Velocity where angle of attack modulation begins (km/s)
  Valpha3 = Valpha1;            % Velocity where angle of attack modulation begins (km/s)
  Vfinal  = 2500*(3.0547e-4);
  CLCDmax=1.4;


%%%%%%%%%%%%%%%%%%%%%%%%%%%%%%%%%%%%%%%%%%%%%%%%%%%%%%%
% Initial conditions for Integration of Equations of Motion
```

```matlab
Vnot = Vnot;                        % User input for initial velocity in km/s
gammanot= gammanot;                 % User input for initial Flight Path Angle (rad)
psinot= psiinit;                    % User input for initial Heading Angle in (rad)
hnot=hnot;                          % User input for initial altitude in km
snot=0;                             % Initial along-track displacement (km)
nnot=0;                             % Initial displacement in North direction (km)
enot=0;                             % Initial displacement in East direction (km)
Longnot= Longinit*(pi/180);         % User input for initial longitude
Latnot= Latinit*(pi/180);           % User input for initial latitude


%%%%%%%%%%%%%%%%%%%%%%%%%%%%%%%%%%%%%%%%%%%%%%%%%%%%%%%
% Integrate the equations of motion
y0=[Vnot gammanot psinot hnot snot nnot enot Latnot longnot];  % Inital conditions
options = odeset('RelTol',1e-7,'AbsTol',1e-10*ones(1,9));
[t,y] = ode45('Re-entryeoms',0:tstep:tfinal,y0,options);


%%%%%%%%%%%%%%%%%%%%%%%%%%%%%%%%%%%%%%%%%%%%%%%%%%%%%%%%%%
% Dummy variables used for plots
totalt=(tfinal/tstep) + 1;          % Dummy variable for use in loops
A=y(:,1);                           % Velocity
B=y(:,2);                           % Flight Path Angle
C=y(:,3)*360/(2*pi);                % Heading Angle
D=y(:,4);                           % Altitude
E=y(:,5);                           % Along track Distance
F=y(:,6);                           % Distance in North Direction
G=y(:,7);                           % Distance in East Direction
L=y(:,8)*360/(2*pi);                % Longitude
T=y(:,9)*360/(2*pi);                % Latitude

end
```

Function used by MATLAB® ODE45to Integrate Equations of Motion

% Reentryeoms

% Equations of motion for planetary re-entry

function [ydot]=Reentryeoms(t,y)

global m Re ge S CD CL H beta rhoe phi psi tstep

global Vnot ydot hnot totalt rohe AoA alpha alphanot psinot

% Guidance

% Velocity Equation

ydot(1,1)= -(1/m)*0.5*CD*S*(rhoe*exp(-y(4)/H))*y(1)^2 -(ge*sin(y(2)));

% Flight path angle with variable density and constant gravity (gamma)

ydot(2,1)= (y(1)/(Re+y(4)))*cos(y(2)) - (ge*cos(y(2)))/y(1)…
        + (1/m)*0.5*CL*S*y(1)*(rhoe*exp(-y(4)/H))*cos(phi);

% Heading angle of Velocity vector equation (Psi)

ydot(3,1)= -(1/(Re+y(4)))*y(1)*cos(y(2))*sin(y(3))*tan(y(9))…
        + (1/cos(y(2))) * (0.5*(1/m)*CL*S*y(1)*(rhoe*exp(-y(4)/H)*sin(phi)));

% Altitude Equation

ydot(4,1)= y(1)*sin(y(2));

% Along-track Distance Equation (in along track direction)

ydot(5,1)= y(1)*cos(y(2));

% Ground Distance Equation (in North direction)

ydot(6,1)= y(1)*cos(y(2))*cos(y(3));

% Ground Distance Equation (in East direction)

ydot(7,1)= y(1)*cos(y(2))*sin(y(3));

% Longitude Equation (Lambda)

ydot(8,1)= y(1)*cos(y(2))*sin(y(3))/((Re+y(4))*cos(y(9)));

% Latitude Equation (Theta)

ydot(9,1) = y(1)*cos(y(2))*cos(y(3))/(Re+y(4));

Excerpt from Trajectory Ooutput Data File

Time	Velocity	FPA (γ)	Heading (ψ)	Altitude (h)	Grnd Dist (GD)	GD North	GD East	Latitude	Longitude
0	7.60	-0.0100	57.00	122.00	0.00	0.00	0.00	25.00	-140.00
1	7.60	-0.0101	56.97	121.92	7.60	4.14	6.37	25.04	-139.94
2	7.60	-0.0102	56.95	121.85	15.20	8.28	12.74	25.07	-139.88
3	7.60	-0.0104	56.92	121.77	22.80	12.43	19.11	25.11	-139.81
4	7.60	-0.0105	56.90	121.69	30.40	16.58	25.48	25.15	-139.75
5	7.60	-0.0106	56.87	121.61	38.00	20.73	31.85	25.18	-139.69
6	7.60	-0.0107	56.84	121.53	45.60	24.89	38.21	25.22	-139.63
7	7.60	-0.0108	56.82	121.45	53.20	29.05	44.57	25.26	-139.57
8	7.60	-0.0110	56.79	121.36	60.80	33.21	50.93	25.29	-139.50
9	7.60	-0.0111	56.76	121.28	68.40	37.37	57.29	25.33	-139.44
10	7.60	-0.0112	56.74	121.19	76.00	41.54	63.64	25.37	-139.38
:	:	:	:	:	:	:	:	:	:
:	:	:	:	:	:	:	:	:	:
400	**6.50**	**0.0158**	**43.91**	**74.59**	**2956.00**	**1858.30**	**2290.60**	**41.46**	**-115.77**
401	6.50	0.0156	43.87	74.69	2962.50	1862.90	2295.10	41.50	-115.72
:	:	:	:	:	:	:	:	:	:
:	:	:	:	:	:	:	:	:	:
799	3.47	-0.0157	30.72	55.17	5094.20	3549.30	3591.40	56.49	-98.19
800	**3.45**	**-0.0154**	**30.70**	**55.12**	**5097.70**	**3552.30**	**3593.20**	**56.52**	**-98.16**
801	3.44	-0.0150	30.67	55.06	5101.10	3555.20	3594.90	56.55	-98.13
:	:	:	:	:	:	:	:	:	:
:	:	:	:	:	:	:	:	:	:
1199	0.10	-0.9781	27.23	11.38	5590.20	3983.10	3831.80	60.36	-94.09
1200	**0.10**	**-0.9788**	**27.23**	**11.29**	**5590.30**	**3983.10**	**3831.80**	**60.36**	**-94.09**
1201	0.10	-0.9794	27.23	11.21	5590.30	3983.20	3831.80	60.36	-94.09
:	:	:	:	:	:	:	:	:	:
:	:	:	:	:	:	:	:	:	:
1398	0.04	-1.0123	27.18	0.52	5597.20	3989.30	3835.00	60.42	-94.04
1399	0.04	-1.0124	27.18	0.49	5597.20	3989.30	3835.00	60.42	-94.04
1400	0.04	-1.0124	27.18	0.45	5597.20	3989.30	3835.00	60.42	-94.04

Integrate Equations of Motion for Hard Coded C_L/C_D Changes

```matlab
%%%%                    Reentryeoms
%  3-D equations of motion for planetary reentry


function [ydot]=Reentryeoms(t,y)
global m Re ge S CD CL ClCd CLnot CDnot H beta rhoe phi tstep
global Vnot ydot hnot totalt rohe AoA alpha alphanot psinot


%Guidance
%  3-D Velocity Equation
if t < 400
   CD = 1.3;
   ydot(1,1)= -(1/m)*0.5*CD*S*(rhoe*exp(-y(4)/H))*y(1)^2 -(ge*sin(y(2)));
elseif t >= 400 & t < 800
   CD = .244;
   ydot(1,1)= -(1/m)*0.5*CD*S*(rhoe*exp(-y(4)/H))*y(1)^2 -(ge*sin(y(2)));
elseif t >= 800 & t < 1200
   CD = .892;
   ydot(1,1)= -(1/m)*0.5*CD*S*(rhoe*exp(-y(4)/H))*y(1)^2 -(ge*sin(y(2)));
else
   CD = 1.3;
   ydot(1,1)= -(1/m)*0.5*CD*S*(rhoe*exp(-y(4)/H))*y(1)^2 -(ge*sin(y(2)));
end


% 3-D Flight path angle with variable density and constant gravity (gamma)
if t < 400
   CL = .8;
```

```matlab
    ydot(2,1)= (y(1)/(Re+y(4)))*cos(y(2)) - (ge*cos(y(2)))/y(1) +
(1/m)*0.5*CL*S*y(1)*(rhoe*exp(-y(4)/H))*cos(phi);
elseif t >= 400 & t < 800
    CL = .336;
    ydot(2,1)= (y(1)/(Re+y(4)))*cos(y(2)) - (ge*cos(y(2)))/y(1) +
(1/m)*0.5*CL*S*y(1)*(rhoe*exp(-y(4)/H))*cos(phi);
elseif t >= 800 & t < 1200
    CL = .655;
    ydot(2,1)= (y(1)/(Re+y(4)))*cos(y(2)) - (ge*cos(y(2)))/y(1) +
(1/m)*0.5*CL*S*y(1)*(rhoe*exp(-y(4)/H))*cos(phi);
else
    CL = .8;
    ydot(2,1)= (y(1)/(Re+y(4)))*cos(y(2)) - (ge*cos(y(2)))/y(1) +
(1/m)*0.5*CL*S*y(1)*(rhoe*exp(-y(4)/H))*cos(phi);
end

%  Altitude Equation
ydot(4,1)= y(1)*sin(y(2));

%  Along-track Distance Equation (in along track direction)
ydot(5,1)= y(1)*cos(y(2));

%  Ground Distance Equation (in North direction)
ydot(6,1)= y(1)*cos(y(2))*cos(y(3));

%  Ground Distance Equation (in East direction)
ydot(7,1)= y(1)*cos(y(2))*sin(y(3));
```

APPENDIX C
ALGORITHM TO PLOT AIR DENSITY

```matlab
function plot_air_density
% Plot the density of the Earth's atmosphere (in kg/m^3) as a function
%   of altitude from 122 km to sea level.

global hnot rhoe rho H D x

% limits of altitude (m)
  start_altitude = 0;
  end_altitude = hnot;
  rhonot = rhoe;                % density of air at sea level (kg/m^3)
  scale_height = H;             % scale height of the Earth's atmosphere (in meters)

% Walk through the range of altitude, calculating the density at
  for (i = 1 : length(D))
     altitude = D(i);
     rho(i) = rhonot * exp(-altitude/scale_height);
  end

  figure(14), clf;
  semilogx(rho, D, 'b');
  xlabel('Density of air (kg/m^3)');
  ylabel('Height above sea level (m)');

end
```

Bibliography

1. Bate, Roger R. and others. *Fundamentals of Astrodynamics*. New York: Dover

2. Chapman, Dean R. "On the Corridor and Associated Trajectory Accuracy for Entry of Manned Spacecraft into Planetary Atmospheres," *AIAA Selected Reprint Series*,

3. Emmanuel Trelat, "Optimal Control of a Space Shuttle, and Numerical Simulation," Report to the Fourth International Conference on Dynamical Systems and Differential Equations, Wilmington NC, May 2002

4. Gerry J. Gilmore. "Space is important to U.S. national security," *The Kwajalein Hourglass,* April 23, 2005

5. Griffen, M. D. and French, J. R., Space Vehicle Design, American Institute of Aeronautics and Astronautics, Washington, D. C., 1991.

6. Harpold, J.C., and C.A. Graves. *Shuttle Entry Guidance*, AAS Paper 78-147, American Astronautical Society, Anniversary Conference, 25th, Houston, Tex., Oct. 30-Nov. 2, 1978.

7. Hartunian, Richard A. "Ballistic Missiles and Reentry Systems: The Critical Years". *Crosslink: The Aerospace Corporation Magazine of Advances in Aerospace technology*, Winter 2003.

8. Hicks, Kerry. Class lecture, MECH 637, Astrodynamic Re-entry. Department of Aeronautics and Astronuatics, Air Force Institute of Technology, Wright-Patterson AFB OH, Winter 2005.

9. -----, "Simple Modeling Tools for Force Application Reentry Vehicles". Phillips Laboratory, OLAC-PL/XPS, California, June 1993.

10. Jenkins, Dennis. *Hypersonics Before the Shuttle*. Washington, D.C., NASA Monographs in Aerospace History, No. 18, June 2000.

11. Marshall Space Flight Center. "X-37 Demonstrator to Test Future Launch Technologies in Orbit and Reentry Environments." n.pag. http://www1.msfc.nasa.gov/ NEWSROOM/background/facts/x37. 29 January 2004.

12. NASIC mil Web Site. *The Mission and Vision.* http://www.wpafb.af.mil/naic/history. html, 2005

13. Philip J. Klass, "CIA Reveals Details of Early Spy Satellites," *Aviation Week And Space Technology*, June 12, 1995, Publications, Inc., 1971.

14. Regan, Frank J. and Anandakrishnan, Satya M. *Dynamics of Atmospheric Re-entry*. Washington DC: American Institute of Aeronautics and Astronautics, Inc., 1993.

15. Shaw, M.A., J.L Carlin and J.D. Adams. "Executive Summary of Analyses of the Space Maneuver Vehicle (SMV)." Report to Space and Missile Systems Center Air Force Materiel Command, Los Angeles Air Force Base, CA. September 2000.

16. Stanford University, "Overview of Policy, Market and Technology Options for Commercial Reusable Re-entry Satellites", June, 1989

17. Vinh, Nguyen X. and others. *Hypersonic and Planetary Entry Mechanics*. Ann Arbor:The University of Michigan Press, 1980.

18. Wiesel, William E. *Spaceflight Dynamics*. Boston: The McGraw-Hill Companies, Inc., 1997.

19. Wikimedia Encyclopedia, *Apollo 15 Command Module*, http://en.wikipedia.org/wiki/Apollo Command/Service_Module, 2005.

20. -----, *Project Gemini*, http://en.wikipedia.org/wiki/Gemini_program, 2005

Vita

Senior Master Sergeant Charles A. Bilbey graduated from Samuel Clemens High School, Schertz Texas in 1979 and enlisted in the Air Force on 1 Apr 1980. After completing basic training at Lackland and Airframe Repair technical training at Chanute AFB, IL. Sergeant Bilbey began his military career as an Airframe Repair Specialist.

Sergeant Bilbey received a Bachelor of Science degree in 1993 from Embry Riddle Aeronautical University in Aerospace Science Technology. He spent 18 years in Aircraft Structural Maintenance, ending that part of his career with the F-16 depot at Hill AFB, UT., where he managed the Air Forces only F-16 Crash Damage Repair Program and eventually assumed duties as the Aircraft Maintenance Production Superintendent.

In January of 1998 after 18 years as an Aircraft Maintenance Master Technician, sergeant Bilbey was accepted for retraining into the 1C6X1, Space Systems Operations career field. He graduated, with honors, as a Distinguished Graduate from the Enlisted Space Operations Training course at Vandenberg AFB, CA. He again visited Vandenberg to attend the training for Early Missile Warning and reported to the 11 Space Warning Squadron, Schriever AFB, CO as a Space Operations Flight Chief on 10 Oct 98. In Apr 2002 Sergeant Bilbey was selected as the Ops Superintendent for the 2d Space Warning Squadron (SWS) and assigned to Buckley AFB, CO.

In May, 2003 sergeant Bilbey was one of 12 members selected for the Enlisted-to-AFIT program to pursue the Graduate of Space Systems degree program at the Air Force Institute of Technology, Wright-Patterson AFB, OH. Upon graduating sergeant Bilbey will join the team at the SBIRS System Program Office at Los Angeles AFB, CA.

<table>
<tr><td colspan="3" align="center">REPORT DOCUMENTATION PAGE</td><td>Form Approved
OMB No. 074-0188</td></tr>
</table>

REPORT DOCUMENTATION PAGE		*Form Approved* *OMB No. 074-0188*

The public reporting burden for this collection of information is estimated to average 1 hour per response, including the time for reviewing instructions, searching existing data sources, gathering and maintaining the data needed, and completing and reviewing the collection of information. Send comments regarding this burden estimate or any other aspect of the collection of information, including suggestions for reducing this burden to Department of Defense, Washington Headquarters Services, Directorate for Information Operations and Reports (0704-0188), 1215 Jefferson Davis Highway, Suite 1204, Arlington, VA 22202-4302. Respondents should be aware that notwithstanding any other provision of law, no person shall be subject to an penalty for failing to comply with a collection of information if it does not display a currently valid OMB control number.
PLEASE DO NOT RETURN YOUR FORM TO THE ABOVE ADDRESS.

1. REPORT DATE *(DD-MM-YYYY)* 13 September 2005	2. REPORT TYPE **Thesis** Master's Thesis	3. DATES COVERED *(From – To)* Oct 2003 – Sep 2005

4. TITLE AND SUBTITLE INVESTIGATION OF THE PERFORMANCE CHARACTERISTICS OF RE-ENTRY VEHICLES	5a. CONTRACT NUMBER
	5b. GRANT NUMBER
	5c. PROGRAM ELEMENT NUMBER
6. AUTHOR(S) Bilbey, Charles A. Jr, SMSgt, USAF	5d. PROJECT NUMBER
	5e. TASK NUMBER
	5f. WORK UNIT NUMBER

7. PERFORMING ORGANIZATION NAMES(S) AND ADDRESS(S) Air Force Institute of Technology Graduate School of Engineering and Management (AFIT/ENY) 2950 Hobson Way WPAFB OH 45433-7765	8. PERFORMING ORGANIZATION REPORT NUMBER **AFIT/GSS/ENY/05-S01**

9. SPONSORING/MONITORING AGENCY NAME(S) AND ADDRESS(ES)	10. SPONSOR/MONITOR'S ACRONYM(S)
	11. SPONSOR/MONITOR'S REPORT NUMBER(S)

12. DISTRIBUTION/AVAILABILITY STATEMENT
APPROVED FOR PUBLIC RELEASE; DISTRIBUTION UNLIMITED.

13. SUPPLEMENTARY NOTES

14. ABSTRACT

When a non-US spacecraft reenters the Earth's atmosphere, having the ability to accurately determine its performance characteristics is a primary concern. This study investigated the atmospheric re-entry profiles of a maneuverable re-entry vehicle. The re-entry vehicle was modeled as a point mass with aerodynamic properties. Equations of motion were numerically integrated, giving the time histories of position, velocity and flight path angle. The algorithm is able to generate a complete and feasible entry trajectory of approximately 25-minute flight time in about 5 to 10 seconds on a desktop computer, given the entry conditions and values of constraint parameters. This preliminary study shows the feasibility of identifying and further exploring the technical challenges involved in using a mathematical model to simulate the performance characteristics of the maneuvering re-entry vehicle.

15. SUBJECT TERMS
Atmospheric Re-entry, Maneuvering Re-entry Vehicle, Re-entry Profile

16. SECURITY CLASSIFICATION OF:			17. LIMITATION OF ABSTRACT	18. NUMBER OF PAGES	19a. NAME OF RESPONSIBLE PERSON Dr. Richard G. Cobb
a. REPORT U	U	U	UU	85	19b. TELEPHONE NUMBER *(Include area code)* 937-255-3636 x45559

Standard Form 298 (Rev. 8-98)
Prescribed by ANSI Std. Z39-18

Form Approved
OMB No. 074-0188